MECHANICAL PROPERTIES INVESTIGATION OF ADDITIVE MANUFACTURED TI-6AL-4V CELLULAR STRUCTURE

by

Husain Alnaser

A thesis submitted to the faculty of
The University of Utah
in partial fulfillment of the requirements for the degree of

Master of Science

Department of Metallurgical Engineering

The University of Utah

May 2018

The University of Utah Graduate School

STATEMENT OF THESIS APPROVAL

The thesis of **Husain Alnaser**

has been approved by the following supervisory committee members:

Ravi Chandran	, Chair	**3/15/2018** Date Approved
Krista Carlson	, Member	**3/15/2018** Date Approved
Ashley Spear	, Member	**3/19/2018** Date Approved

and by **Manoranjan Misra** , Chair/Dean of

the Department/College/School of **Metallurgical Engineering**

and by David B. Kieda, Dean of The Graduate School.

ABSTRACT

Ti-6Al-4V is an alloy that has been developed to be used in medical implants due to its compatibility with the human body. Additive manufacturing technology has also become useful in constructing human bone design (marrow) from Ti-6Al-4V, imitating bone function. This research focuses on studying mechanical properties of Ti-6Al-4V using powder laser bed fusion (PLBF).

This thesis describes the lattice structure for Ti-6Al-4V and discusses the design and the properties of the material based on tensile testing and other tests. This thesis focuses on understanding the mechanical properties of Ti-6Al-4V by presenting a literature review and comparing the structural strengths of the lattice and the full solid. Then, the research examines the powder comprising the fabricated specimen, the design that was chosen, and the parameters that affect the design mechanical properties in the results.

Also, part of the discussion discusses heat affected zones (HAZ) comparing welding to additive manufacturing (AM) as a micro-weld. This section reveals some of the answers about the variability of mechanical properties in AM technologies, especially in PLBF.

Lastly, microstructure images and CT scan images were analyzed through Image J. The image processing helps relate theoretical data and experimental results to

quantitative data acquired from image processing. After compiling the analyses from the various sources, a design model was created to enhance the investigation of mechanical properties by giving visual evidence to support the conclusions.

TABLE OF CONTENTS

ACKNOWLEDGMENTS

First, I thank God for all the blessings and opportunities that He has given me. Also, I thank Him for all accomplishments I obtained thanks to His delicate care and direction in my life.

Second, I thank my family for their moral and financial support whenever I needed it, especially my father Faisal Alnaser and my brother Falah Alnaser. Without their great help and effort, this research would not have existed. I also thank my mom Zakia Althaleme, who prays for me every day for good fortune and luck while waiting for my return to celebrate my achievements.

Third, I am grateful for my advisor Dr. Ravi Chandran for helping me constantly whenever I needed assistance and guiding me through the research by offering his expertise and labs to aid my research. Also, I thank Dr. Ashley Spear for her dedicated effort and discussions that helped me understand my research from a different perspective. I thank Dr. Carlson for improving the quality of my thesis.

Fourth, I thank Dr. Anthony Sanders from Ortho development for providing me specimens at no cost to conduct my research. Also, I thank my colleagues Ahmed Degnah, Somnaang Rou, and Alexander lark.

Lastly, I thank everybody who I forgot who helped me in any way. I pray from the bottom of my heart for them to be healthy, wealthy, and happy

CHAPTER 1

INTRODUCTION

1.1 About AM

Additive manufacturing (AM) technologies (AMT) give several methods to manufacture a part using different types of materials. AMT can use different materials, such as metals and alloys, and combinations of different materials to build a structure. In addition, AM has few limitations regarding geometry complexity; consequently, much attention has been drawn towards this technology. The time- and cost-savings of AM are also significant. It saves time by replicating designs and changing them based on customer demands regarding size and material. These demands are based on the needs of customers such as dental implants where each tooth is different in size and shape. In addition, for jewelry, people have different hand sizes and hence different ring sizes to fit their finger that can also be costumed by AM. Also, it only uses the material required to construct the desired structure; in other words, AM dramatically reduces the machining required to produce the final structure, saving the powder for building another part. AM-structure resolution depends on the technology and the particle powder size used to fabricate the structure. Common AM technologies, electron beam melting (EBM) and laser bed fusion (LBF), can also be compared. Electron beam melting has a higher

resolution than laser bed fusion, and the power usage is less efficient. Regarding powder size, smaller powder size correlates to better resolution but worse flowability. Also, an important parameter is powder sphericity, because spherical powder tends to flow better. [1]

Many questions can be asked about AMT concerning fabrication, material selection, and materials design. A basic knowledge is mentioned in the upcoming chapters to help explain the process through discussing key concepts. Many names for a porous metal structure refer to the same concept such as foam metals, cellular structure, and lattice structure. Foam metals are porous structures that have a repeated *uniform* unit cell. The uniformity of these unit cells originates from repeating a certain geometry to produce the part, such as a brick in a wall. These unit cells have many designs, shape, and size differences based on the application. Some of the designs even purposely have random porosity arrangements. The main purpose of fabricating metal foam is to achieve an ultra-lightweight material with high strength. [2]

1.2 Applications

Metal foams have many applications, such as heat sinks for electronics, air filters, and joint and bone supporters, and the AMT foam structure has become commercially available because it can be easily manufactured with a chosen material. Also, AMT minimizes the powder feed material used, because it is possible to exactly control what to build without any excess material attaching to the designed structure. Therefore, titanium matrix composite (TMC) has become an option for use in applications that need high compressive loadings. TMC has superior mechanical properties to other composites such

as polymers honeycomb reinforced with carbon fibers in terms of sheer strength. [3]

Powder metallurgy plays a large role in the mechanical properties of foam structures, and powder characteristics influence the resolution, composition, surface finish, and strength of the structure fabricated. For example, finer powder particles provide higher resolution and increased strength, but there are several limitations. When the size of the particle decreases, the flowability also decreases, as mentioned previously. Also, it becomes harder to clean the machine. Regarding composition, using powders dramatically improves alloy fabrication through AMT. For example, making superalloys is almost impossible through casting/addition of materials, but by using powder, superalloys can be made. [4]

Surface finish (SF) mainly depends on the particle size. A smooth SF can be obtained through machining, but to reduce the cost and the time for machining, it is better to decrease powder particle size to fabricate with an acceptable to good SF. Decreasing the powder particle size also increases the strength of the part fabricated after it is sintered due to the densification vs. course particle size relation, and these results are discussed further in the Discussion chapter. Coating the parts also strengthens the structure fabricated. Some coatings also enhance wear resistance and protect against corrosion depending on the application environment. [5,6]

1.3 Initiation of Interest

A study performed by Dr. Spear and her graduate students in the Mechanical Engineering Department at the University of Utah shows a variation in mechanical properties for parts that were printed by laser bed fusion (LBF) vs. invest casting for

aluminum alloy 6061. Aluminum alloy 6061 consists of manganese, magnesium, iron, titanium, zinc, silicon, and chromium. [7] The comparison was based on compression testing for these printed parts. Figure 1 graphs force vs. displacement and shows a variability in performance between compression loadings of LBF parts that were printed. As the part initially starts from the zero position when it gets compressed, the specimen shrinks in the Z-direction, and that is considered the +Z direction.

1.4 Properties Variability

An analytical view investigates more about why variability occurs between the two printed parts through tomography imaging while the parts are compressed. Figure 2 shows that there is a difference in behavior at the 4-mm displacement mark for the compressed ligaments structure copy A vs. copy B. The figure also shows that there is a difference in the building structure between the two copies of the ligaments. There are several reasons for this difference. First, powder particles adhered to the wall of the thin

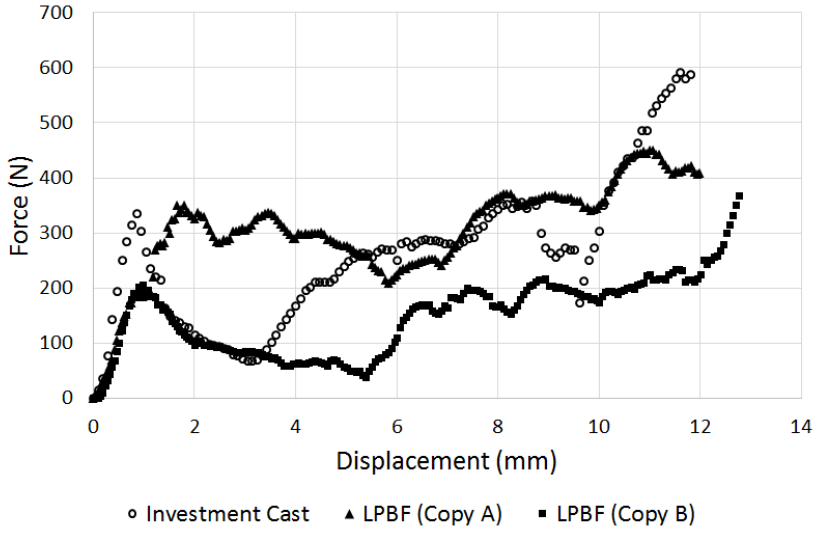

Figure 1: A compression test for the aluminum alloy.

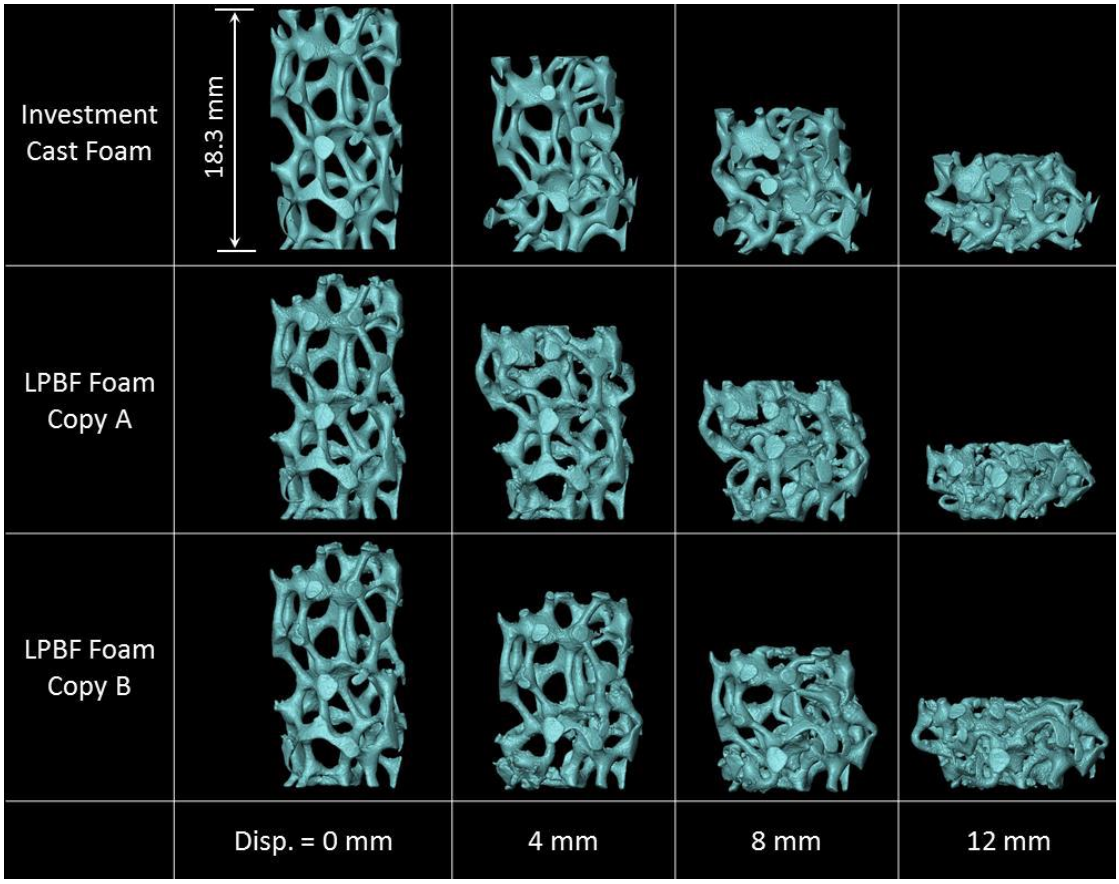

Figure 2: µ-CT Imaging of compressed Al alloy, the focus is on Copy A and B.

ligaments during sintering become fused into the main structure, making the wall rough or bumpy looking, or the adhered powder particles can change the dimensions of the ligaments in a way that distributes stress differently, leading to different failure locations. Second, the design on the computer has a perfect cell structure that gets repeated, but in reality, the cell structure might not get built, or some particles are knocked off by powder particles when the cell structure is evened by the roller. These structure defects can occur due to the lack of fusion and the angle of the structure features. The angles make the fusion used to build the structure either easy or difficult. Vertical angle is the most favored angle for building when going to higher or lower angles of fusion between

particles that are uncompleted in some cases. Third, powder feed for laser bed fusion process does not consist of a new batch of powder. To save money, companies usually mix the feed with new, used, and overflow powder. The problem with that is used powder will have some heating effect from the previous build, possibly changing powder sphericity. If that occurs, resolution, as discussed previously, is affected; therefore, the structure ends up having variation in the parts. A suggestion has been made to make ligaments large enough to eliminate the machine variability during fabrication. Also, enlarging the segment eliminates the problem of powder particles sticking to the walls, because the wall to powder particle size ratio becomes large. In addition, Figure 3 is a close-up view of the ligaments, showing the variability in dimension and reflecting what has been discussed thus far. [8-10]

Lastly, the microstructure of cast aluminum vs. laser bed fusion printed part shows results that must be further investigated. Usually, when having more alloying elements, the powder-based process is better suited to form the alloy. Some alloying elements tend to segregate or dissolve into each other, forming different compositions than anticipated, and this is always the case for superalloys. Therefore, it was proposed in this study that printed parts would have better mechanical properties than casted parts, but the opposite result was found.

1.5 Microstructure of Al Alloy

The microstructure in Figure 4 (a) shows the invest casting specimen and (b) shows the printed part specimen. The invest casting micrograph shows the grain boundaries for different regions in different colors that have equal size distributions

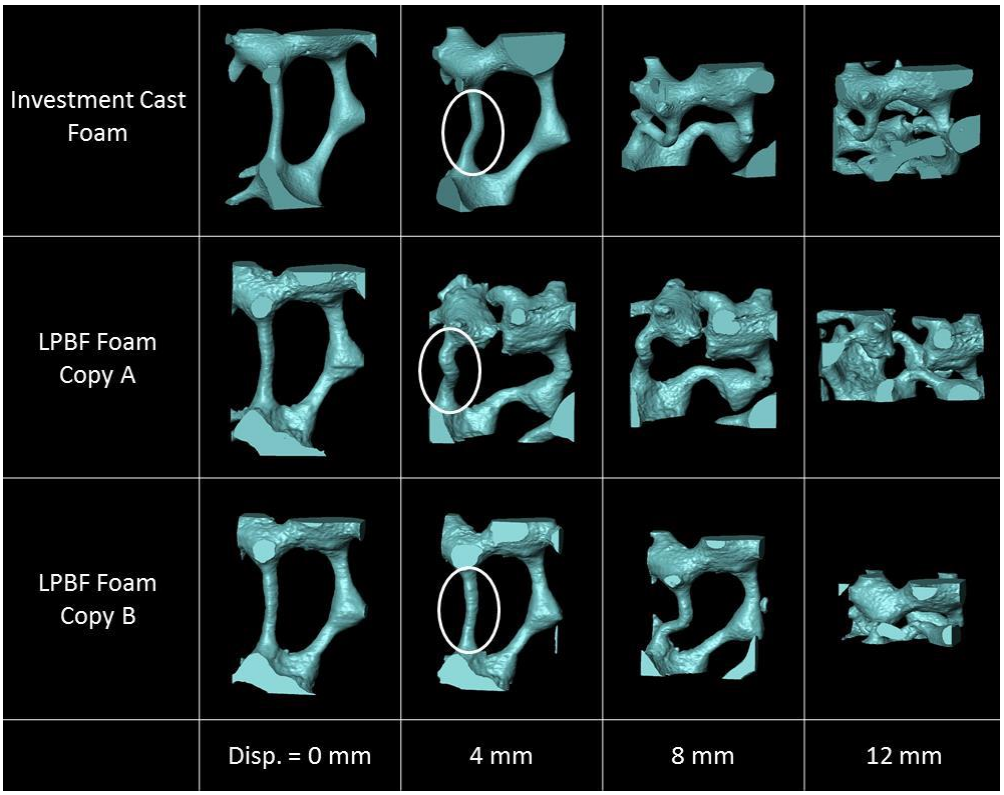

Figure 3: A close-up μ-CT image for compression testing.

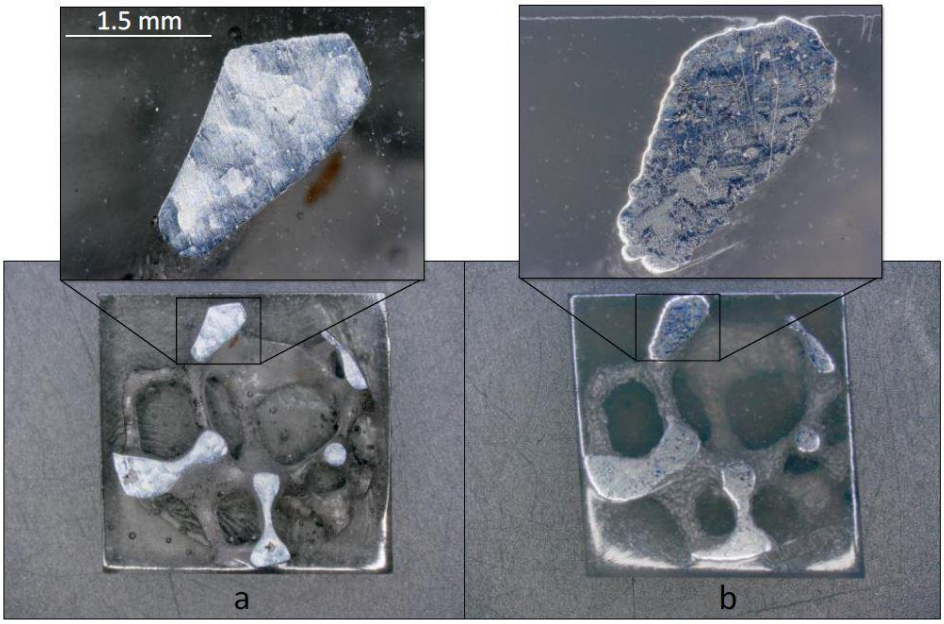

Figure 4: Microstructure of a) cast part and b) AM part.

overall. The printed part micrograph shows some sort of segregation and separation of alloys in the structure, because there was not sufficient time during printing for nucleation to evenly occur throughout the structure. In contrast, there was sufficient time during invest casting for nucleation. Also, printed parts show severe heat affected zones (HAZ). Usually problems appear within that zone; consequently, the smallest welds show the best mechanical properties. Corrosion first attacks these zones, and making small welds is the common welding process.

Finally, since HAZ are active, there is a good possibility of growing pores within the structure ligaments, leading to easy fatigue crack initiation and then failure. This focuses on compression tests; therefore, it does not show the tensile testing performed on these specimens to further investigate the hypotheses. Nonetheless, in general, pores act as regions where stress concentrates, producing an easy path for crack propagation due to stress concentration. [11-14]

1.6 Research Objective

The objective of this research is to acquire an understanding of AM Ti-6Al-4V cellular structure behavior under tensile stress and analyze the data to create a model that can predict AM behavior alloy made of Ti-6Al-4V. In this research, the lattice structure of Ti-6Al-4V formed from powder was analyzed from different angles to clarify the behavior of AM parts, why AM printed parts do not exhibit the same mechanical behavior, and why there is always variation in mechanical properties.

CHAPTER 2

LITERATURE REVIEW

2.1 Background

2.1.1 Alternative Names of AM

There are many names that describe the same process for AM that have been used in the past due to their functionality. The broadest term that is most commonly used is AM. Several of the other names are mentioned and discussed in this work due to the benefits and drawbacks of each name.

Rapid proto-typing was used to indicate an experimental design that can be examined and improved before needing to manufacture the desired structure. The benefit of this name is it emphasizes that the process is fast and repeatable, meaning that more examination can be done on a part. However, the term proto-typing indicates that the part is not finished yet, giving a poor impression even if the part is made perfectly. The term indicates that the part is imperfect, possibly preventing costumers from buying it. [15]

3D printing is mainly the name used for stereolithography, because the term is very easy to digest and to remember. Also, it is catchy for the ears. 3D printing as a name conveys the idea that any structure can be built using 3D printing. However, the drawback of this name is its usage. Companies and manufacturers have associated this

name with stereolithography, and others consequently understand 3D printing as non-metal-based 3D printing. [16]

The term automated fabrication has been used to indicate that manual labor is not necessary because machines do all the work. The benefit of this name is that it describes the process as being fast and free labor; consequently, automated fabrication is cost effective. The drawback of this name is the elimination of any indication of AM, resulting in heavy drawbacks marketing-wise, and the name is particularly unfavorable among commercial consumers, i.e., "anybody who would like to get an AM printer." The name solid freeform fabrication was created to emphasize the geometrical shape complexity, and as it is named *freeform*, it does not need a mold to hold the shape of the fabricated structure. This makes the marketing easier, because not requiring a mold reduces cost. Also, it has the freedom of shape complexity. However, solid freeform fabrication can raise many questions about the material the process uses and the quality of the material fabricated. In particular, using the term fabrication makes the process seem as if it has poor resolution, because the produced structure is fabricated and not manufactured or built. Lastly, regarding the AM name, it is perfect and superior to the above names due to very simple fact of the simplicity and the wide-range applicability of the name. The wide range comes from the understanding that material is being added. Thus, AM can be complex and fast and any material can be used. In addition, AM indicates that the quality is good, and the name is technical, showing some embedded technology in it. [17]

2.1.2 Description of AM Components

AM has a preference for using components that need to be built; therefore, it is advised to know about capabilities and potential drawbacks. AM technology is perfect for small complex geometrical designs. In contrast, for large parts, it is still better to use casting and other techniques. AM is best for small parts mostly because it can accommodate very high shape complexity and material complexity. The main drawbacks for AM technology relate to the material powder used and design orientation. Material powder needs to be processed to have one size for use in an AM machine to produce a uniform bed, because the quality of the material is dependent on the quality of the material powder used. Powder sphericity plays a major role in flowability by making the powder flow easier so no clogging occurs in the feed system and preventing particle agglomeration. Also, powder contamination levels can play a major role in fusion and cause weak fusion or intermetallic compounds that are not favored, causing failure to the part while testing. As for the orientation of the design, it can sometimes be tricky and obnoxious. The Discussion chapter of the thesis discusses this matter further. In this thesis, the printing of tensile specimens is horizontally oriented. Printing them vertically may cause design deficiencies where the top layer may get tipped by the blade or powder particles that are being evenly spread by the blade or the roller knocking a lower powder particle to cause a tilt in the structure, resulting in shape disposition. Thus, building parts horizontally is advised. Also, it is more efficient in terms of time and cost. [18]

2.1.3 Direct vs. Indirect AM

Indirect AM is not common due to the production of green parts. Green parts refer to parts that are brittle and very sensitive to motion that thus need to be sintered to make them tougher for handling and machining forces encountered during stereolithography and binder jetting procedure.

Stereolithography is a layer-by-layer technique that cures a photosensitive resin using ultraviolet (UV) light. After the design is finished, the design is sintered. During binder jetting, a binder is sprayed through ink-jet printer nozzles to glue a layer of metal powder; then, the next layer is added until the design is finished and then sintered. [19]

2.1.4 Design Complexities for AM

There are four types of complexities that must be considered when designing parts to be printed by AM technology: shape, hierarchy, function, and material complexities.

Regarding shape complexity, AM has no limitation on shape complexity, because any shape can be manufactured with AM technology, and an example would be a cellular structure such as bones. Regarding hierarchical complexity, AM can change sizes of the build based on the designer desires. An example would be parts for fighter jets, because they can have different opening sizes. For functional complexity, AM can build a design that needs assembly in one build. Similar to ball bearings, AM needs an assembly, but the design can be built in one run with AM structures. Regarding material complexity, AM has a wide range of material choices, since the part can be built by one of two ways, point by point or line by line, and the materials can be elements or alloys. Currently, Ti-6Al-4V is used in research widely due to its various uses and commercial availability. [20,21]

2.1.5 AM vs. Reverse Engineering

Reverse engineering is the process of tracing a finished structure back to its origin to acquire the blueprint of the finished structure for modification or reproduction. Optical 3D scanning is the most common and cheapest technique used. It is faster than other techniques, but it cannot scan anything beyond the surface. Consequently, if geometrical designs exist inside the structure such as a piping net, they cannot be scanned. Computed tomography (CT) scan is perfect for scanning internal structure using X-rays. However, it is expensive and slow, since it goes layer by layer. In addition, the size of the object to be scanned must be small; otherwise, the amount of data will be too large for a computer to maintain and process for later stages. [22-24]

2.1.6 AM vs. CNC

Computer numerical control (CNC) machining is exactly the opposite of AM function-wise. AM builds layer by layer until the design is finished, while CNC extracts layer by layer until the design is finish. CNC material loss is greater than AM, making AM more valid to use for expensive materials. Both technologies have advantages and disadvantages, and they are summarized in Table 1.

If the shapes are simple, CNC machining is a better choice and is faster than AM in producing the design. As the complexity of the shape increases, the AM process becomes more preferred. Regarding accuracy, it is a variable of shape complexity. CNC program has more tools to select from, meaning more options are available to machine the design. [25,26]

Table 1: Comparison between CNC and AM based on advantages and disadvantages.

Advantage/Disadvantage	AM	CNC
Speed	Bad	Good
Complexity	Good	Bad
Accuracy	Depend on Geometry	Depend on Geometry
Programming	Bad	Good

2.1.7 Lattice Material vs. Fully Dense Material Comparison

The comparison presented in Figure 5 performed by the University of Virginia graphically shows the strength vs. density of various materials. [27] According to the graph, the density of a foam material is 10^0, while the density of a full material is approximately 10^1, showing that the full material is denser than the foam version of the same material by approximately 10 times. The strength of the foam material is approximately $10^{1.5}$, while the strength for full metal strength is 10^3, meaning that full metal is approximately 30 times stronger than foam metal.

2.2 Method of Fabrication

2.2.1 Open and Closed Foam Structures

An open cell structure refers to a structure with open space where a line can be drawn from one side to another without touching the structure walls. In contrast, a closed cell structure refers to a structure with closed space where a line cannot be drawn from one side to another. An easy way to distinguish between the two structures is by taking CT scan images and visually analyzing one slice of the CT scan, as shown in Figure 6.

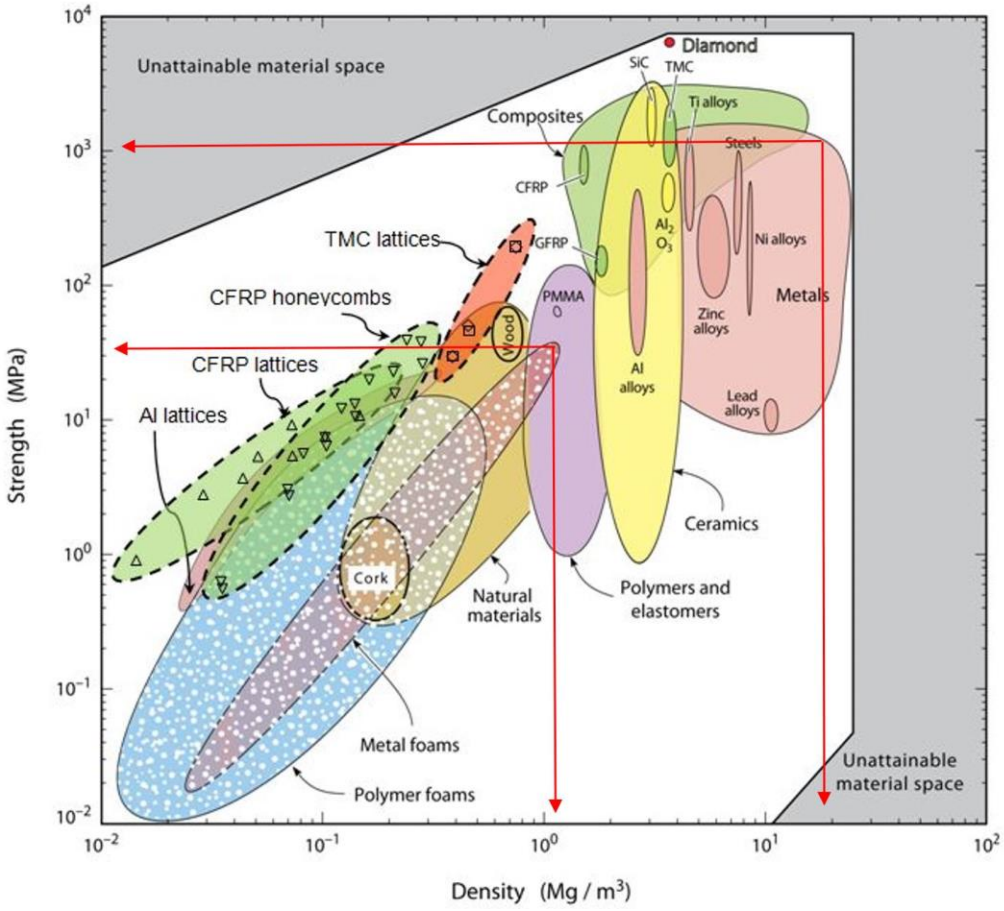

Figure 5: There are many reasons to determine the structure that is needed based on the application. [27]

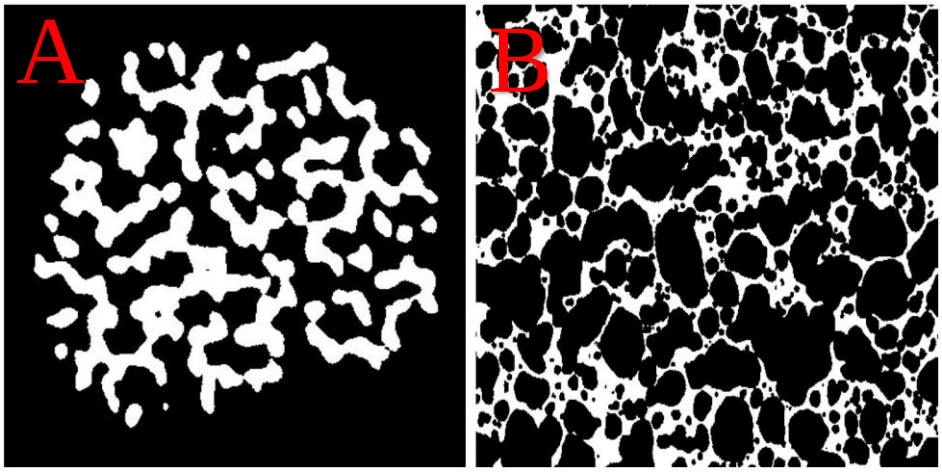

Figure 6: Images of CT scanning for different structure types. a): An image of Ti-64 CT scanned showing open structure “black color is connected” Figure 6 b): An image of concrete CT scanned showing closed structure “black color is not connected” [28]

Black color represents void and white color is solid material. If a line is drawn through each image, a line goes through Figure 6 a), while a line does not go through Figure 6 b).

2.2.2 Foam Fabrication

There are novel processing techniques to produce a porous structure, and each process contains different steps and requirements for fabrication. The goal is to provide an idea about other techniques that were used before AM became commercially available, and the major techniques are discussed in this work.

The bubbling technique uses a molten metal alloy bubbling inert gas to give foam structure its shape and to ensure the gas does not react to the molten metal. This technique is used in making some aluminum alloys, as shown in Figure 7.

After adding the bubbling agent, adding a metal hydride to a molten metal while stirring makes a mix that results in foam structure. The mix is heat treated to release hydrogen gas, expanding the alloy. This technique is used to produce closed foam cells, and it is famous for producing an aluminum foam structure using a titanium hydride agent. By adding leachable particles to the metal powder, a foam structure is then formed. The process involves mixing the metal/alloy powder and a leachable material powder that can produce an open foam cell when leached. These are the basic ideas of making foam materials without using AM technology. There are more techniques for forming foam materials that have not been mentioned, but since the goal of this discussion is only to show that techniques other than AM can produce foam material, there was no need to go through the details of the processes. Figure 8 gives a basic understanding of the processes that can be used to produce cellular structure and its type (open/closed).

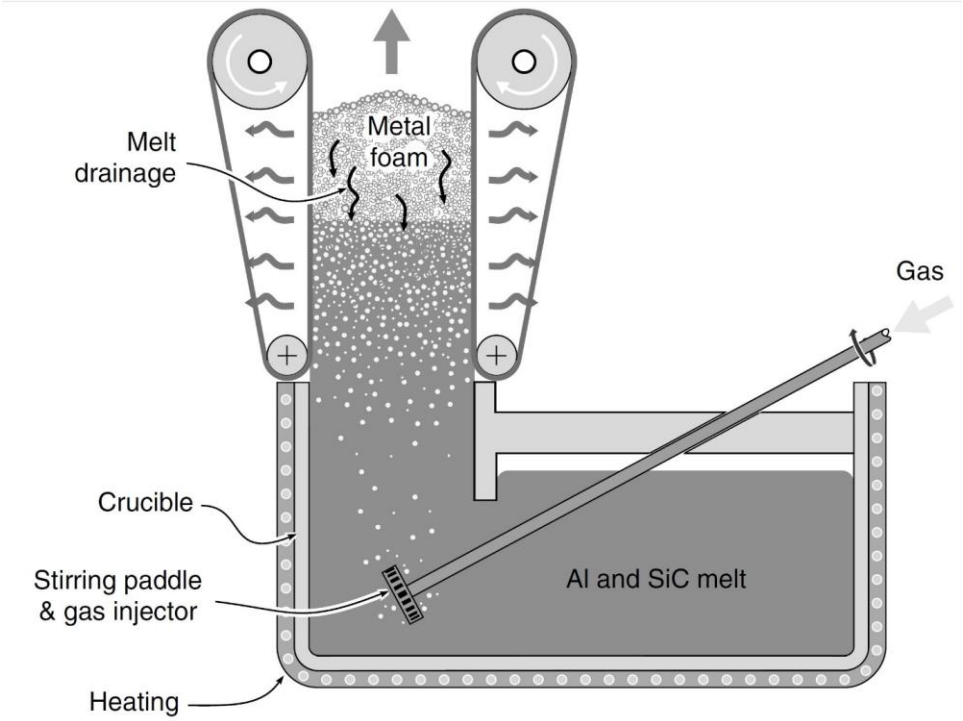

Figure 7: A schematic of the melt gas injection of Al-SiC. [29]

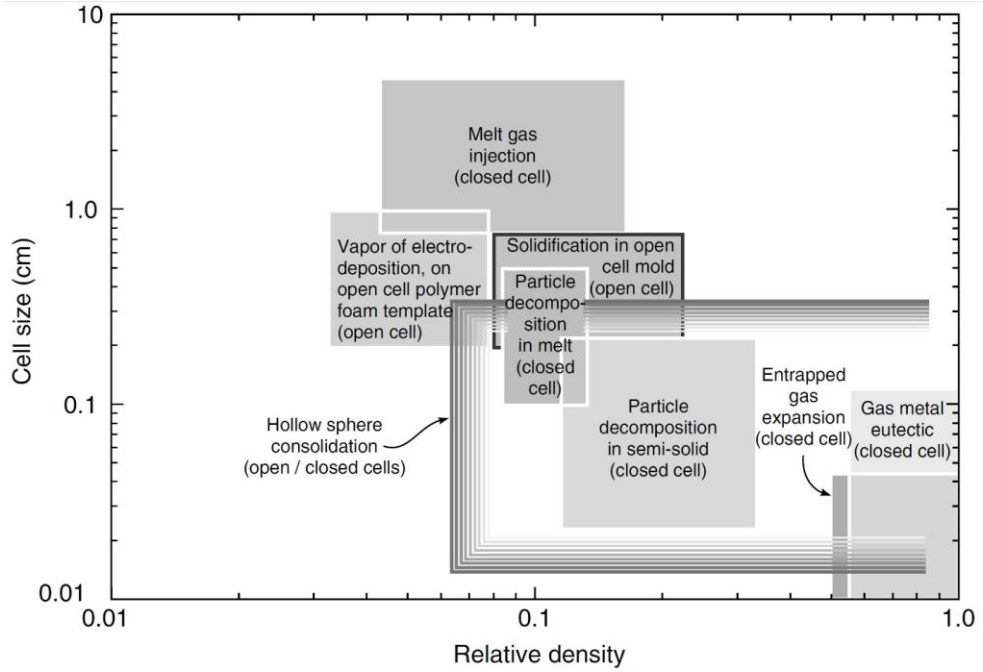

Figure 8: A graph that shows some process that companies use to produce foam materials. The graph gives an estimate of density vs. cell size based on each process. Figures 7 and 8 are from the same source. [29]

2.2.3 AM Equipment

Companies using AM technologies use various types of equipment based on the design size, complexity, and material that must be fabricated. This section briefly discusses other equipment that can be used to fabricate three-dimensional structures, and powder laser bed fusion (PLBF) is discussed thoroughly in section 2.4.1.

There are three basic methods used to categorize AM technologies. First is the use of material powder and source of heat. This method is the most common due to its high resolution relative to other AM technologies. Also, it is fast and works with small parts. If the design is larger than 50 cm, this technique becomes impractical due to the long time needed to build the design. Examples of alternative techniques are PLBF and electron beam melting (EBM). [30]

Second, there are some technologies that use a resin mixed with the powder. The mix then is cured by UV light or laser to solidify the resin and to prepare it for the next stages. This technique requires post-heat treatment to remove the binder material from the design, and then heat treatment can be initiated to complete the process. An example of vat photopolymerization (VP) is presented in Figure 9. Most photopolymer resins have at least two different photo imitators, because higher rates of polymerization indicate that the design parts can be built faster. In addition, it is done by changing the concentration of the initiators. However, the resulting polymer has reduced weight by the same factor. Acrylates have better photo speed and better flexibility than epoxies, but it has a high shrinkage rate of 5–20%. Epoxies, in contrast, are the total opposite; they are stronger than acrylates and shrink about 1–2% but have lower photo speed. Therefore, a mixture of acrylates and epoxies is used to give optimum usage for the process. Some benefits

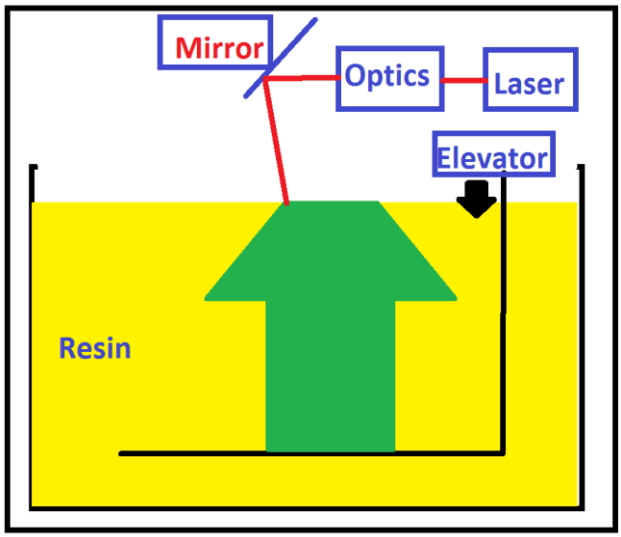

Figure 9: A schematic of a typical VP process. The process progresses layer by layer until the design is done. When one layer is built, the elevators make the designed structure go down one layer so it can continue building the design structure.

of VP are surface finish range from submicron to 100 micrometers and the flexibility to support many machine configurations of different machine frames and size scales. In addition, large build volumes are possible. Some negatives for VP are the usage of photopolymers, limiting the use of acrylates and epoxies because chemistries are limited; the polymer aging, leading to degradation in the mechanical properties of the fabricated structure over time; the current material not having good qualities in terms of durability and strength; and the process requiring post-curing. [31]

The last method is the usage of a binder. A binder works similar to resin, but the process is different. The binder is mixed with the metal/alloy powder to produce support. Afterwards, heat treatment with lower temperatures is required for debinding, possibly elevating the temperature for powder sintering and making the starting temperature the same as the temperature of the final process so the process progresses from the step of debinding to sintering without cooling or stopping between the processes. The

mechanisms of printing the part include point by point like binder jets and fused deposition modeling, as shown in Figure 10. [32,33]

2.2.4 AM Name Synonyms

There are several names used to describe foam structure based on the method of fabrication used. Each name has its own uniqueness, and some of the names that have been used in the manufacturing of foam are presented in this section.

> Cellular metal is the most general term, referring to a metallic body in which any kind of gaseous voids is dispersed. The metallic phase divides space into closed cells which contain the gaseous phase.
>
> Porous metal is a special type of cellular metal restricted to a certain type of voids. Pores are usually round and isolated from each other.
>
> Solid metal foam is a special class of cellular metals that originate from liquid-metal foams therefore, it has a restricted morphology. The cells are closed, round, or polyhedral and are separated from each other by thin films.
>
> Metal sponge is a morphology of a cellular metal, usually with interconnected voids. [34]

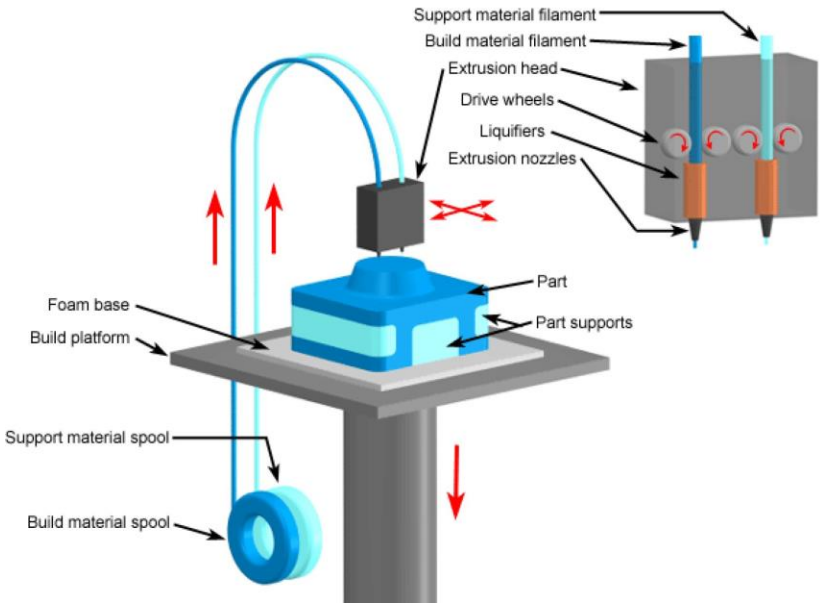

Figure 10: A schematic of the filament-based fused deposition process. [17]

2.2.5 AM Tree

There are several ways to produce metal foam, and Figure 11 summarizes the ways of foam metal fabrication depending on gas usage during the process.

A method to fabricate foam structure is through machining to produce the closed cell honeycomb structures in Figure 12. Thus, a roll of metal is drawn through two rolls with a star shape so the material pulled from them has a zig-zag shape. Then, these zig-zag sheets are placed on top of each other to form a closed foam structure. Another way is using punches to make holes in the sheet and then placing another die with a single punch to give a zig-zag shape. Then, the shapes are stacked to form a foam structure with a truss-like structure. [36,37]

2.2.6 AM vs. PM

The first step in PM is determining the composition of the powder material and then determining the desired characteristics for further processing. Generally, fine, spherical powders are the best for the AM tech to use because sphericity enhances flowability and gives max packing density. Regarding particle size, particles

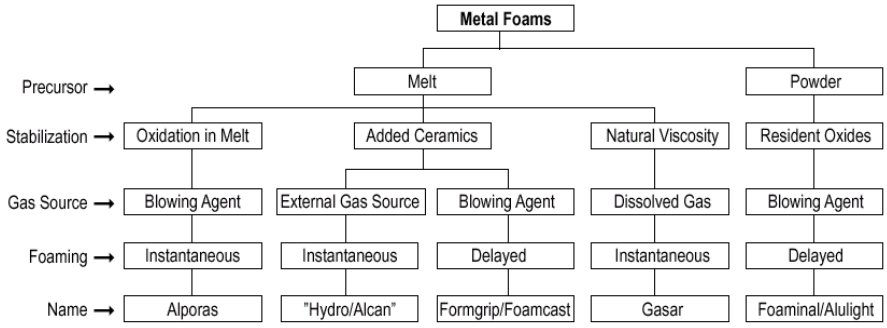

Figure 11: The main ways of metallic foam fabrication, through powder and through melts. The route is chosen depending on the alloy that needs to be fabricated. Thus far, this research has discussed the powder route. [35]

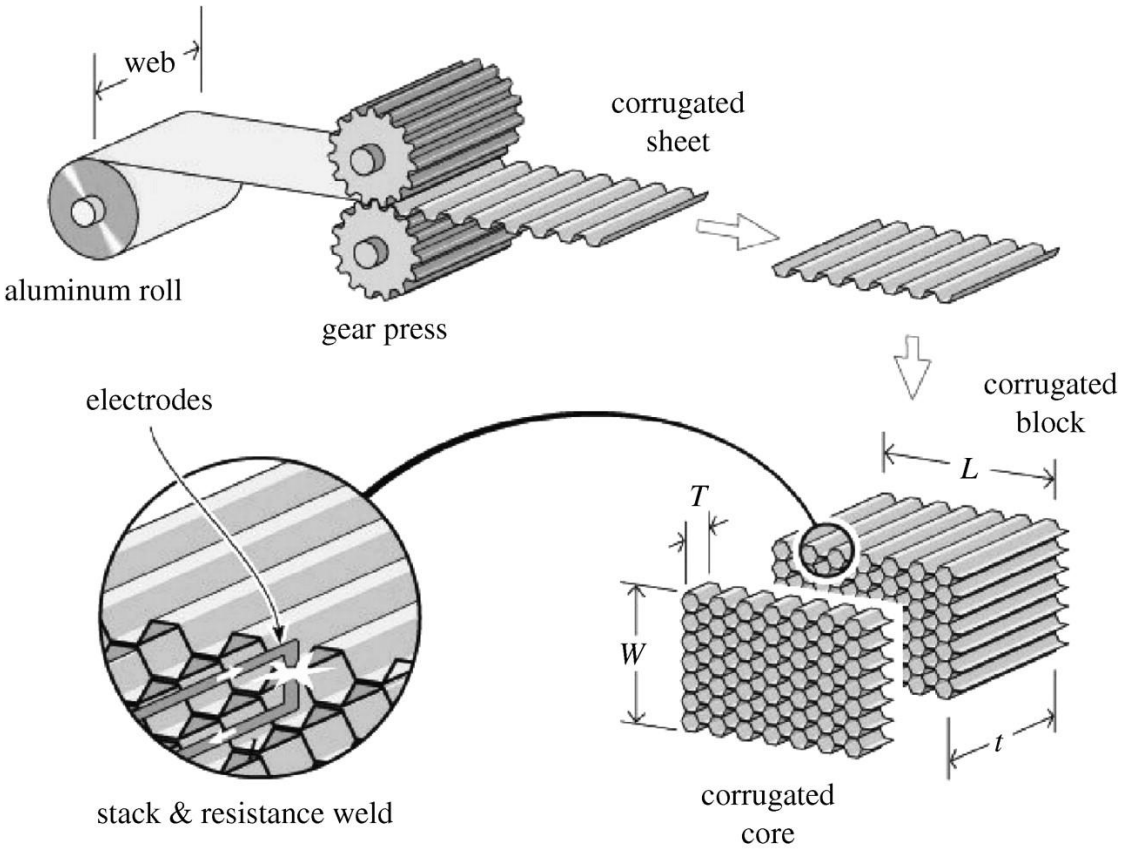

Figure 12: A schematic of the closed-cell honeycomb structure process.

size affects retaliation and the sintering process. Afterwards, there are two pathways to reach green density, using a PM process or an AM process. A PM process uses high pressure to form the part and the part is moved to the sintering process area. In contrast, an AM path uses laser, ink, and binder techniques to reach the green density part and then sends it to be sintered.

Sintering then occurs to densify the part, and in case of binder existence, sintering is necessary to presinter the part to debind the binder. (Optional step.) Lastly, hipping is used to reach the final desired density, because the part is ready to be used at this point. Another optional step is surface refining; it can be done to further improve the quality of

the surface because of the nature of AM surface parts. It is required to have a substrate to prevent warpage of the build due to high internal stress in AM produced parts, while PM produced parts do not require a substrate. The primary benefit of AM is that it allows modification of the powder size, granting better surface finish and higher accuracy. The powder size can be fine, but the flowability decreases as the powders size decreases. This tradeoff affects both AM and PM parts. In addition, maintenance of PM equipment is relatively easy and fast compared to AM equipment. [38]

To compare AM to PM, a case study of Ti-64 has been performed using a PM process to study the effect of temperature and time on parts made out of fine and coarse powders. The importance of this study is to help explain the major factors that can affect sintering to improve the AM processes.

2.3 Case Study of Ti-6Al-4V

2.3.1 Powder Metallurgy (PM) Summary History

Titanium manufacturing began in the late 1940s with sponge titanium and vacuum arc re-melting; however, powder techniques were mostly abandoned. The 1980 minerals, metals and material society (TMS) conference drew large attention to titanium PM techniques such as blended elemental and complex shape production. This, in turn, sparked large interest in researching titanium powder metallurgy. Within the last decade, interest in AM methods to produce near net shape titanium alloy parts has skyrocketed mostly due to the advances in computer technology. If current trends hold, AM may be the dominant production method for expensive metal alloys such as titanium. PM can be separated into three main steps. First, powder preparation consists of mechanical

techniques, atomization, and electrical/chemical methods. Second, powder shaping or forming consist of pressing, binder extrusion, injection molding, and pressure and temperature consolidation. Third, sintering and consolidation consisted of sintering in inert gas, sintering in vacuum, liquid phase sintering, and microwave sintering. [39]

2.3.2 Experiment Objective

Heat treatment greatly benefits an alloy if performed appropriately. Therefore, a study was performed to analyze the effect of heat treatment on Ti-64 with two different powder sizes, coarse and fine powders, by using the time and temperature as variables.

2.3.3 Experiment Procedure

Starting with the powder preparation process, the initial powder, 20/60 reading alloy titanium hydride granules, was ball milled for 30 minutes, sieved for 45 minutes with 100 and 400 mesh, and mixed for 1 hour with added 6Al-4V master alloy. Ball milling was used to produce the powder shown in Figure 13. There were 24 structures produced; 12 were fabricated using course powder, and 12 were fabricated using fine powder.

Flowability, particle size, and Brunauer–Emmett–Teller (BET) tests were performed. The flowability was very difficult to test, because the fine powder flowability was very poor. Finer powders correspond to low flowability, because powder tends to agglomerate due to static and van der Waals forces. The test depends on particle movement through an opening that is narrow. This technique did not work when powder clogs the opening while course powder in use. Therefore, an alternative method

Figure 13: The ball milling containers.

was used. The method is to pour the powder, forming a cone, and then the needed angle to comprise a *repose angle* was calculated. Then, the flowability was calculated.

The particle size analyzer was used to determine the particle normal distribution. The technique is easy and convenient to use; only one gram of material powder needs to be mixed with water that flows in a tube. The tube is transparent, letting light travel through it. A laser beam is sent through the tube, and when the particle appears, the particle blocks the laser; at the other end, the detector will get the reading to producing a normal size distribution. However, if two particles stick together, they are read as one particle. Also, if a particle is oriented vertically, the particle blocks the laser beam and is read as a large particle, but the particle might only have a flake shape. Therefore, it is recommended to run the test to double check and exclude the irregularities that might occur.

2.3.4 Experiment Compaction Method

After finishing the characterization of the powders, the next step is taking the powders to a uniaxial hydraulic press, and the final product is shown in Figure 14. This step consists of several mini-steps that are very important, and any mistake in any step will result in failure of part compaction. First, all the equipment that is going to be used must be prepared and cleaned from previous use to ensure that they are clean so the dies can perform properly, avoiding loss of force on the walls of the dies. For example, the die can be lubricated with a very thin film to ensure that no powder escapes from the sides when pressing. During powder preparation inside the die, the die must be tapped several times to make the powder even. Performing this step helps prevent any defect and makes the press occur as planned. Tapping appears to be the key to fabricating a successfully even part that has uniform thickness, and this has been observed after observing several parts that have been made using this process. [40]

Figure 14: The die and other assisting equipment used to build the part. The pressure used was around 49–50 Short tons.

2.3.5 Experiment Sintering Method

Sintering is required after powder compaction to strength the green parts that have been produced, and the process is shown in Figure 15. Sintering densifies the part by making the particles bond together, and for this study, sintering was performed at different temperatures and times. There are several things to consider while sintering. The atmosphere must be controlled to minimize the chance of the part having any defects. Controlling the atmosphere while sintering can prevent oxidizing, can achieve reduction in the part, or can be a carbon control reaction. Vacuum is also a possibility for atmosphere manipulation. [41]

2.3.6 Experiment Measurements Method

After sintering the part, the shrinkage rate can be calculated by taking measurements. Therefore, taking measurements before and after sintering is required to perform calculations. For volume measurement, the Archimedes method was applied where the part is submerged in water resulting in the displacement of water due to the buoyancy force surface of the part. The method gives a reading that is sensitive to small bubbles that might attach to the surface of the part. It is advised to wash the part with distilled water and then submerge the part in distilled water to eliminate the possibility of bubbles sticking to the surface. Bubbles can increase the buoyancy of the part, resulting in lighter weight and introducing error to the calculation. Also, it is better to measure the water temperature for more accurate results.

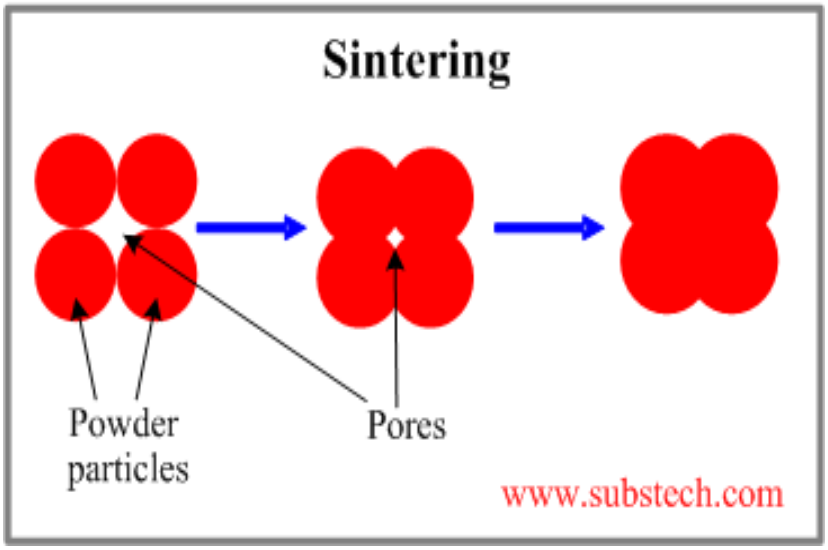

Figure 15: Schematic showing powder densification while sintering. [42]

2.3.7 Experiment Optical Preparation

After taking sample measurements, the samples were engraved with numbers, cut with a disk saw, and mounted for polishing preparation. There were polishing grits with 400, 600, and 800 grits used to prepare the samples for fine polishing. Fine polishing was conducted by applying alumina slurries of 1 micrometer and 0.08 micrometer on the samples. Then, etching was performed to prepare the samples for optical microscopy.

2.3.8 Experiment Results

Table 2 shows that fine powder parts were affected by temperature elevation more than time, while course powder parts were affected by time more than temperature elevation. The distribution of powder particles must be considered while sintering, because the distribution affects compaction and sphericity. However, in this case study, the assumption is both powders have the same sphericity factor but they have different sizes.

Table 2: Experiment summary.

Conditions	Volume Reduction (%)			
	1100 °C, no dwell	1200 °C, no dwell	1200 °C, 30 min.	1200 °C, 4 hours.
Fine	25.12	29.26	26.73	27.44
Coarse	17.16	17.05	22.54	28.82

2.3.9 Experiment Microstructure

The same conclusion produced from the previous test can be seen in the micrographs of Figures 16 and 17.

2.4 Powder Laser Bed Fusion (PLBF)

2.4.1 Mechanism

AM machines add up material layer by layer until the desired design is completed, and PLBF follows the same procedure and has the same major components as other AM machines. The starting point is from a powder delivery system where it provides powder to the powder bed by using a roller or similar equipment to evenly distribute powder on the powder bed. Then, a heat source (in this machine, the heat source was a laser) is applied to the powder, melting it to build the first layer. Then, the piston in the Z-direction is moved one layer down to allow the other layer to build after the roller evens a new layer above the first layer. This process continues until the design is complete, and any excess powder is pushed by the roller to be collected in the overflow container. [43]

It is important to understand how parts can be produced using PLBF to prevent any defects from occurring. There are several parameters that control the error margin, and the biggest parameter that affects the build is powder.

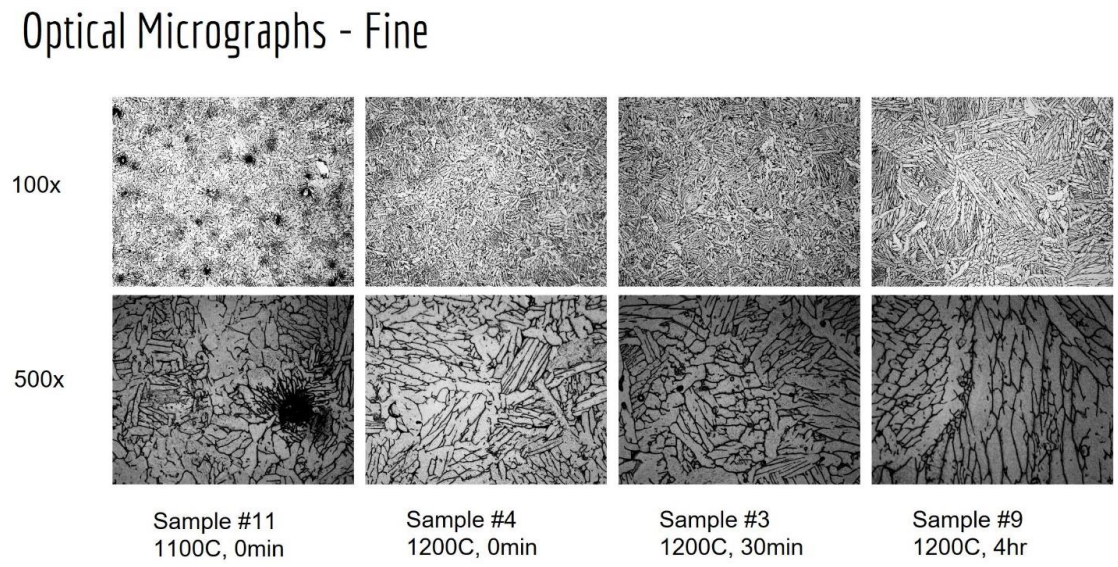

Figure 16: Optical image comparisons of fine powders samples.

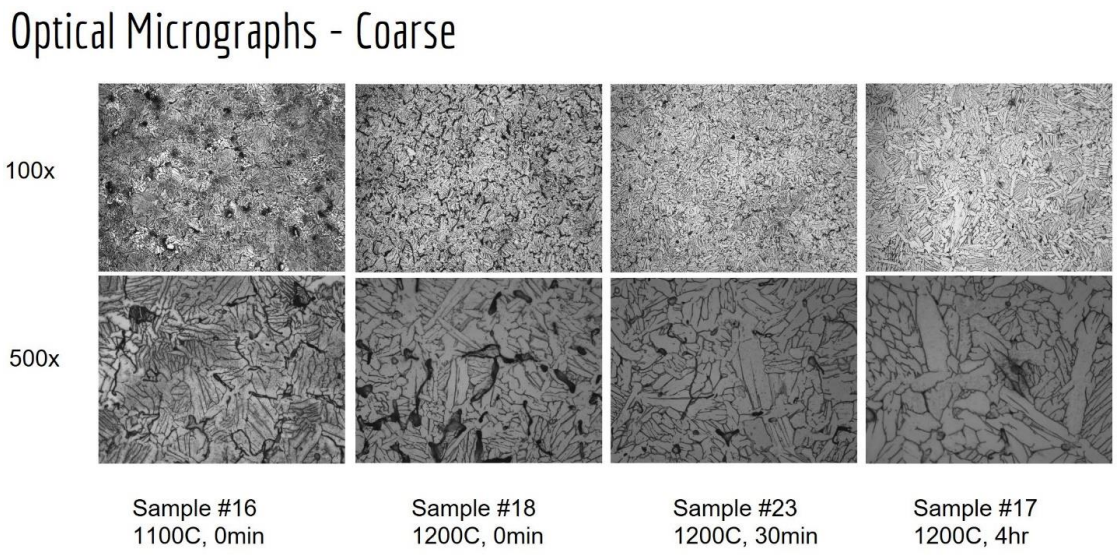

Figure 17: Optical image comparisons of coarse powders samples. All results refer to the same source. [40]

2.4.1 Rule of One Third (1/3) for Powder

Companies use the rule of one third (1/3) when using powder. The rule is that the powder is a mix of the following three types of powder: new batch powder, overflow powder, and whatever is left in the powder bed area. They all get mixed and used for other parts, and a schematic of this process is presented in Figure 18. This process cuts down the cost of using new powder every time a part needs to be printed, since the powders of some materials are expensive.

The problem associated with this rule is that each powder is slightly different in structure, influencing the production of the parts that are fabricated. Consequently, no two printed parts exhibit the exact same mechanical properties. [44]

For example, a part can be built from only pure iron powder. This part will show excellent mechanical properties compared to other powder types. As for the overflow powder, there is a chance that it will become contaminated by the surrounding atmosphere. Lastly, the powder bed area powder has been influenced by heat during fabrication, resulting in possible microstructure change, sphericity of the powder change, and thermal stress. Therefore, when all powders are mixed together and used for building another part, the presence of a defect is greater. Consequently, good heat treatment is advised, but it will not solve the problem completely. In addition, if an alloy is used, the probability is even greater. [45]

There are other parameters to also consider such as laser intensity, laser width, scan speed, and building pattern. These parameters play a role in fabrication as well.

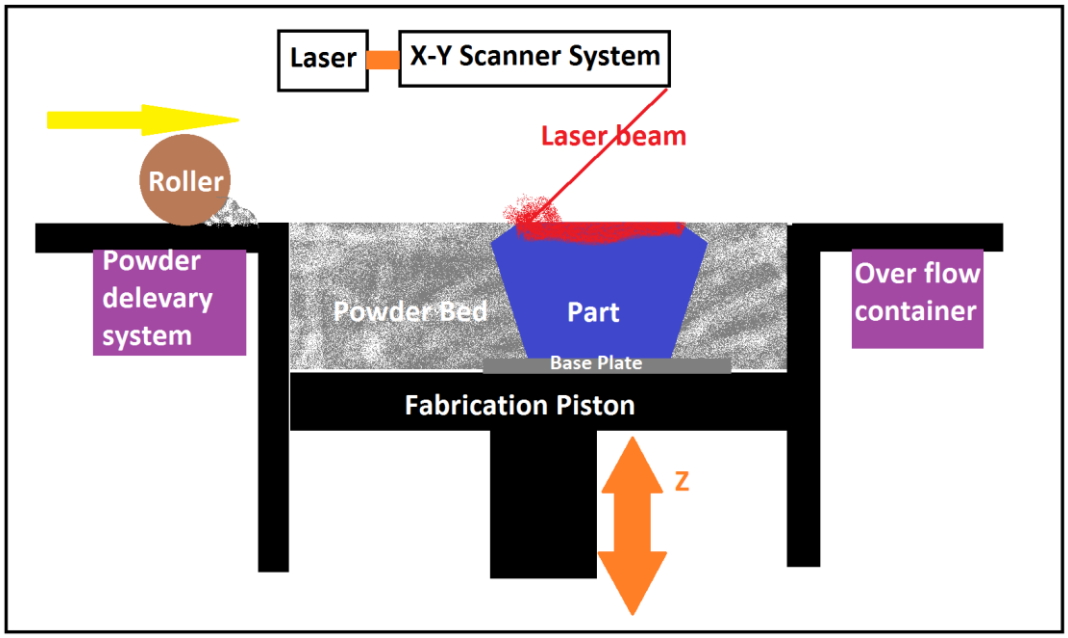

Figure 18: A schematic of PLBF.

2.5 Heat Affected Zone (HAZ)

As discussed briefly in the aluminum alloy case study, HAZ produces many defects to the parent material if not performed with caution and precession, and a schematic of HAZ is shown in Figure 19. HAZ is defined as the area that is affected by heat due to the wielding that occurs near it. This term HAZ is widely used in welding articles and studies. The problem with this phenomenon is the microstructure change caused by heat elevation/cooling. Heating the grain of a microstructure increases the size of the grain, leading to poor mechanical properties and making that region prone to chemical attack, corrosion, crack formation, and any other mechanical failure. Therefore, many solutions have been proposed and confirmed to overcome this problem. For example, one solution is making the weld material corrosion resistant or even have improved mechanical properties from the parent material so the zone is stronger and that mechanical/chemical failure does not reoccur in the same zone. Another solution is to

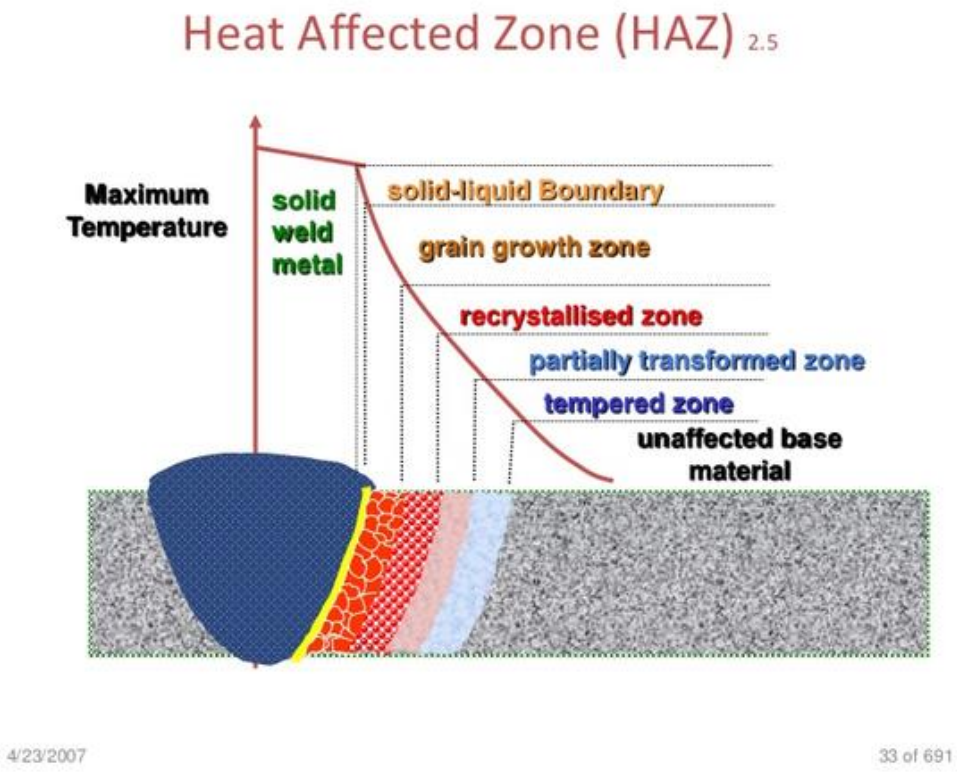

Figure 19: Heat affected zone diagram.

decrease the area of wielding and make it as small as needed to get the job done; by doing that, the HAZ size is smaller than traditional welding techniques, and this HAZ is called a micro-weld. [46]

PLBF uses a laser to print the part in the micro-weld process. Therefore, HAZ has a great effect on the structure, and it must be investigated and never be neglected. The process of AM can be developed to minimize the effect, or another technique can be used to avoid creating HAZ zones such as using binder jetting technology.

CHAPTER 3

MATERIALS AND METHODS

3.1 Equipment

One of the most important pieces of equipment to do mechanical testing is the material testing system (MTS) machine, as shown in Figure 20. The machine can perform tensile testing, compression testing, and fatigue testing. With each test, the setup must be changed, and the program corresponding to each test must be calibrated. For tensile testing, the machine applies tension forces until the specimen fails. For compression testing, the machine applies compressive forces to the specimen until the specimen fails. For fatigue testing, the machine applies oscillation movement under a load to initiate cracks until the specimen fails. There are several grips that can used, and several fixtures can be used to hold the specimen.

A diamond saw cutter was used to cut the specimens, because they are relatively soft. In addition, a diamond saw cutter has been used to cut some of the support structure and to cut the specimen to prepare small pieces to be used later for obtaining optical microstructure and high magnification microstructure by SEM.

Optical microscopy was used to capture microstructure images to compare and analyze. The optical images provide the research direction and determine what other tests

Figure 20: Tensile test setup. Two hydraulic grips with two sets of flat fixtures and 1-inch extensometer.

are needed to confirm the hypothesis. Specifically, optical microscopy confirmed the need to use SEM and obtain microstructure images. SEM revealed great details to assess the hypothesis of the research, and different magnifications were used for separate functions. Some magnifications were used to calculate the fracture percentage, while others were used for visual analysis to determine the fracture type that occurred.

The furnace (heat treatment unit) was essential because of the need of applying heat treatment for some of the specimens. The atmosphere was argon controlled to

minimize oxidation levels and to prevent possible hydrogen embrittlement, because titanium in nature binds with hydrogen at elevated temperatures to produce TiH_2.

PLBF was used to produce the specimen structure that was investigated during the research performed by Ortho development. There is no detailed information on the equipment, because these parameters for the equipment are confidential and exclusive to Ortho development.

3.2 Material

The material of interest is Ti-6Al-4V (Ti-64), and Ortho development provided the tensile specimens that were investigated. The processing of making Ti-64 is confidential, but its raw form was powder, and it was fed into the LBF. Therefore, there is no section in this research on powder preparation and mixing, because Ortho development provided the materials.

Regarding alloying, to improve the mechanical properties of a metal, the most common way is by adding other elements to it to enhance the metal performance or to create a phase that is hard to form without adding a stabilizing element. In this case, the base element is Ti and the alloying elements are Al and V. Al is an α stabilizer and it has good ductility and oxidation resistance. V is a β stabilizer, and it has a good corrosion resistance. By adding these two elements to Ti, the alloy created has excellent properties that can be manipulated by heat treatment and cooling rate to increase either phase α or phase β. Also, heat treatment and cooling rate can change the microstructure texture and create several unique microstructures.

3.3 Removal of Printed Parts

At the beginning of the research, the first batch was removed from the substrate by pliers, damaging the side of the tensile bars. Therefore, electron discharge machine (EDM) cutters were used after examining the first few specimens that had geometric defects. In addition, the defect was accounted for in calculations.

3.4 Heat Treatment

Heat treatment has many profiles depending on the end goal. For this research, the goal is to enhance β phase formation to provide good elasticity property and to bind powder particles to the structure, closing all the gaps between powders. Heat treatment conditions were a constant temperature at 1350°C, 8 to 10 hours annealing time, and an argon gas atmosphere.

3.4 Sample Preparation

After mounting the sample, different grit sizes were used to polish the sample to reveal the microstructure in its most clear form, starting with grits 400, 600, 800, 1000, and 1200. Then, alumina powders of 1.0, 0.3, and 0.05 nm were used to mirror finish the sample. Lastly, Krill agent was used to etch the sample to show the microstructure and boundary of the sample.

SEM sample preparation is very critical to make the sample conductive to give good images to capture; otherwise, charging occurs, showing black or dark lines while capturing the image. Also, there is the possibility of the image creeping, which is also a form of charging. Therefore, making the sample conductive is very important to obtain

images that can help the visual analysis of the research.

Tensile testing sample preparation is the key to obtaining accurate results. The sample needs to be filed or cut depending on the part that needs to be removed. Samples that have support structure attached to it need to be cut by the diamond saw. Small protrusions can be leftovers of the support structure removal step; therefore, protrusions need to be filed to maximize fixture grip and to prevent sample slipping.

CHAPTER 4

RESULTS AND DISCUSSION

4.1 Design Inquiries

4.1.1 Unit Cell Structure Design

The research goal is to investigate the mechanical properties of titanium alloy (Ti-6Al-4V) cellular structure for medical applications. The structure is a closed cellular structure that has 12 and 14 sides orientations (Dodecahedron and Tetradecahedron) similar to the structure shown in Figure 21. The design was influenced by bone marrow structure. It is very hard to mimic the structure of the bone because of AM size limits. Therefore, natural foam is the closest structure to mimic bone that can be programmed and built with good resolution to give good mechanical results. The unit cell is made of 6 Tetradecahedron and 2 Dodecahedron mixed in a random orientation to fit 1 inch of gauge length. [48]

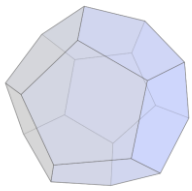

Figure 21: Polyhedron structure, the basic form of Dodecahedron and Tetradecahedron. [47]

4.1.2 Design Development

The application of this alloy is widely spread on different fields due to its properties. The general properties that make this alloy famous are high strength, corrosion resistivity, biomedical compatibility, and high ductility. The cellular structure is built through the laser bed fusion process. This project began with designing a porous structure that was going to be tested by tensile testing. The design simply looked similar to a normal tensile test bar with the exception of the material comprising the gauge length being porous.

The design underwent several stages until it was built. First, the design dimensions and shape were created based on ASTM standard E8. From there, a basic drawing of the sample was created to assimilate the bar that was going to be built, as shown in Figure 22.

The design was completed and ready to be tested, and there were several ideas for the design to enhance the quality of the tensile bar. The batch printed to be tested in each set contained three tensile bars. These sets were built with the same structure but had different designs. Second, the cylindrical design was built in the same batch to be tested against the square design. The square design was better because of the ease of machining after printing, and the design was close to the initial design programmed, allowing for no loss in dimensions and easy set up for tensile testing.

Regarding the cylindrical design, machining flattens one of the sides of the surface, making the test bar geometrically defected. Also, the fixture was not ideal to grab the cylindrical bar, resulting in some unreliable data. The fixture challenge has been adapted to fit the rest of the tensile bars to conduct good results. Therefore, the square

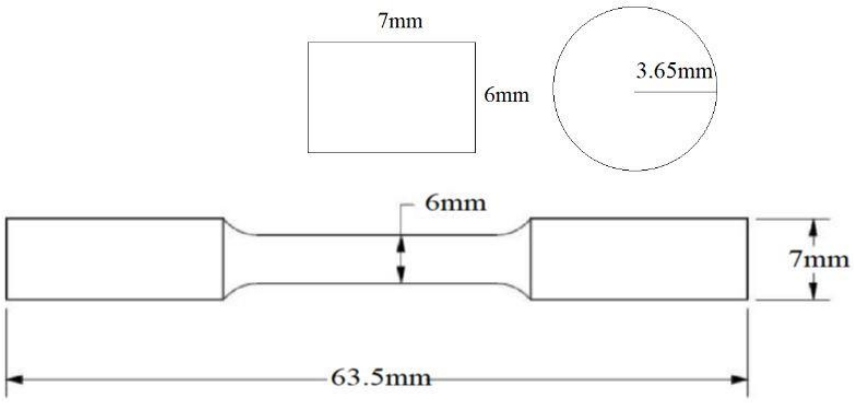

Figure 22: Basic design dimensions of the tensile bar while the gauge length was porous.

design is much more efficient than the cylindrical design.

Third, the sets were printed with different support structure thickness to reduce thermal stresses that are built while printing the tensile bars. Lastly, the last set was built with an extra support structure to reduce thermal stresses, and the sets are shown in Figure 23.

4.2 Mechanical Testing

4.2.1 Tensile Testing

Tensile testing is one of the basic tests that can reveal much about the material tested. Basically, the tensile test compares the force measured by the machine and the displacement measured by an extensometer. Force divided by area gives engendering stress and change of length divided by original length gives engineering strain. By graphing these two parameters against each other, various properties can be determined such as elastic moduli from the slope and ultimate tensile strength from the maximum stress measured. In this research, the investigation focuses on the variability of ultimate

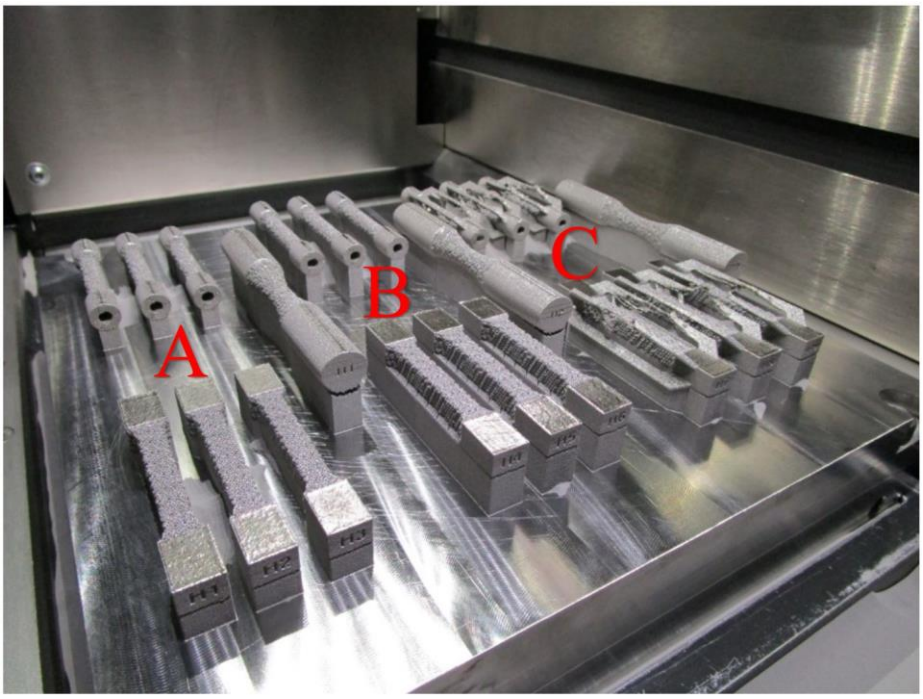

Figure 23: Tensile bars that were printed. (A) Specimens with a basic support structure; (B) Specimens with a thicker support structure; (C) Specimens with a thick support structure + an extra support structure connecting the two-solid base of the structure. The three specimens in the middle of the substrate are fatigue test bars. The round base specimens have a hole in the solid base to reduce thermal stress while printing. For this batch, the idea was tested, and thermal stresses were lower in the round specimens compared to the square specimens.

tensile strength and finding reasons for that phenomenon in metallic additive manufactured parts and suggesting solutions. Therefore, tensile testing was performed to investigate the behavior of Ti-64. The test was performed on three categories of samples: non-heat treated, heat treated well, and overheated samples. The goals of each category are explained in the next section. [49]

Non-heat-treated samples were the starting point of the research where samples can be divided into sub-groups, as mentioned in the Design Section. The purpose of these samples is to obtain a basic understanding of Ti-64 behavior under stress and to compare different heat treatments and determine the best treatment that results in the best alloy

based on the desired task. Also, it gives data for comparison to heat treated samples. Since the structure is unique, acquiring such data is vital to better understand the research findings.

As for heat treated samples, part of the procedure increases ductility and strength by heat treatment, since AM parts are usually fragile; consequently, they only allow handling. Different heat treatments were conducted to investigate the cellular structure tensile strength and compare it with the tensile strength of the original AM parts with no heat treatment. One heat treatment was performed by Ortho development, while the other was performed at the University of Utah.

Finally, the percentage of the surface fractured due to tensile testing was approximately calculated using Image J (image process program). The fracture percentage is proportional to tensile strength; as a rule of thumb, having a larger surface area to resist tensile forces results in higher tensile strength. That is true for most AM parts that have been tested, except for the overheated parts, because the fracture percentage is approximate and does not add up. As for the other samples, the findings are very clear and well stated. Further analysis of the heat treatment is advised to reach a final solid conclusion of the best heat treatment for the AM Ti-64 cellular structure. [50]

The samples show tensile strength variation, as shown in Figure 24 and Table 3. There are several samples that produced strange behavior, for example, showing massive ductility compared to other samples, but this reading is not accurate due to instrumental error caused by sample slippage, resulting in such behavior. Therefore, these data were not reliable, so that they were neglected and were not included in the stress strain Figure 24 due to their error. However, those results wore accounted for, because the results

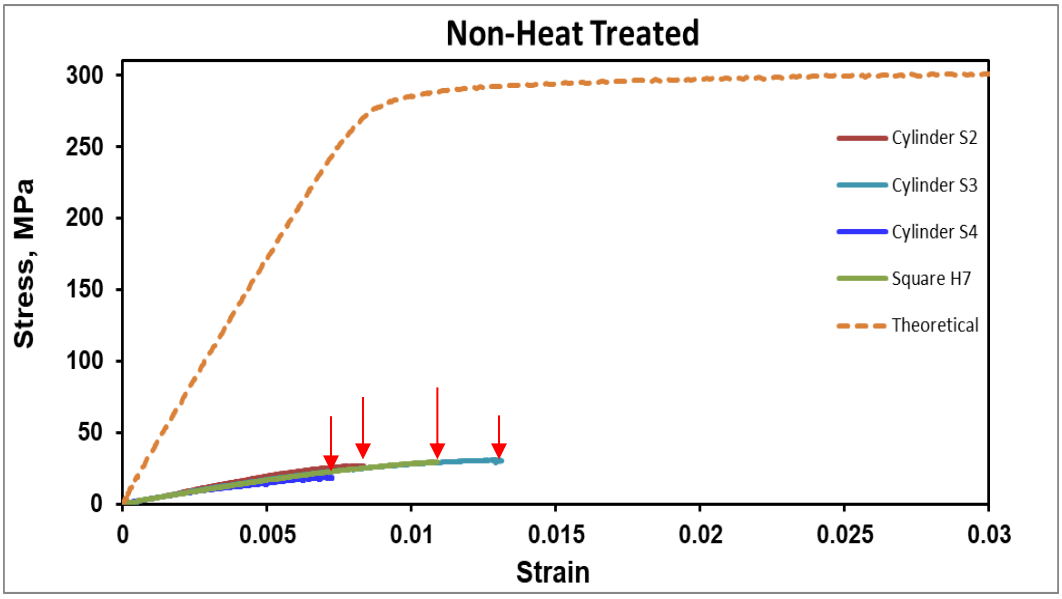

Figure 24: Stress-strain graph for non-heat-treated samples. “S” stands for round base structure sample, and “H” stands for square base structure sample, and the tensile testing was done at the University of Utah.

Table 3: Mechanical properties of samples.

Sample	E (GPa)	σ_y (MPa)	UTS (MPa)	σ_F (MPa)	EL %
S2	3.8	NA	26.65	25.5	0.8
S3	3.3	28.3	30.56	29	1.3
S4	3.2	NA	18.55	18.1	0.7
H7	3.3	28.6	29.45	29	1.1
Theoretical	34	288	307	276.8	14.5

contributed to the discussion on determining the best base geometry for testing. The conclusion was that the square base was better for testing, but the grip fixtures must be changed for better holding. That conclusion was confirmed by observing the defected samples, and the result was helpful in improving the test quality for further samples.

Table 3 shows that samples behave similarly in the elastic region given by the slope (elastic modulus E), but in the plastic region, the behaviors of the samples are different for each sample summarized by the ultimate tensile strength (UTS), fracture

strength (σ_F), and elongation percentage. The suspected reason for the differences between samples is the lack of fusion between powder particles, making the mechanical properties vary.

Samples M1 to Z1 were different from other samples, because the tensile test bar was built to hold three samples at once and then the samples were cut to the proper length by EDM wire. Therefore, each group that was built from the same piece has the same letter. This work assumed that strength is proportional to the fractured area. However, the results from the groups show that assumption is not valid. The reason for that is because each group of tensile specimens came from one big specimen that was cut to the proper size. Consequently, some variability in size and condition of manufacturing clearly influenced the structure. This fact is not essential to this research, since the intention was to test heat treatment. Therefore, the size difference is negligible since it is around 1.5 mm^2, as discussed in the Fracture chapter, and the area of the build has been modeled to form the stress-strain graph. The tensile strength is affected by the area of the material that connects the polyhedron segments. These segments' areas are significant due to the fusion of the powder particles and the thickness of the segment. The goal of overheating was to sinter all the powder and make each segment (truss) of the polyhedron uniform in thickness. The result was good because the segments were uniform, but without the support structure, the cellular structure warped, and the results of the samples that were overheated are presented in Figure 25 and Table 4. For that reason, the quality of heat treatment process was improved for better quality. Figure 26 and Table 5 illustrate the results of the samples that were heat treated with the best heat treatment process determined thus far. [51]

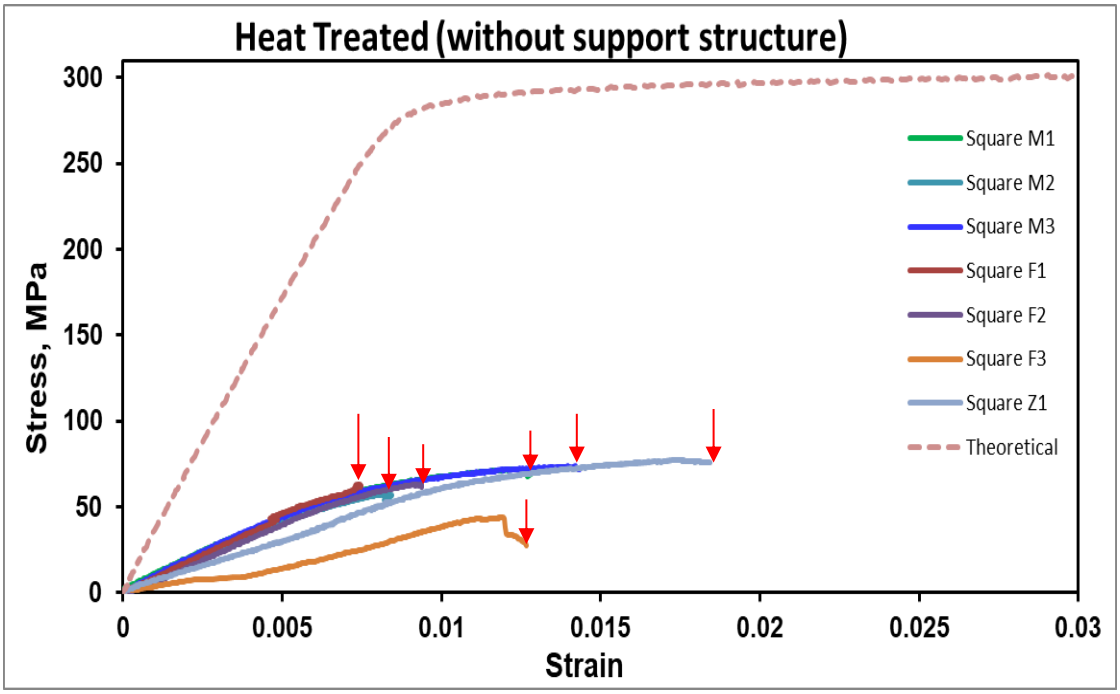

Figure 25: Stress-strain graph for overheated samples (heat treated without support structure). All the samples are square base, and the naming is due to different batch testing performed at the University of Utah.

Table 4: The mechanical properties for over heat-treated samples (heat treated without support structure). Mechanical properties vary in the samples, and as mentioned, the suspected reason to such behavior is the lack of fusion. However, at this point, there is no evidence to support this claim. Later sections of the text show SEM images that show interesting results that are discussed thoroughly to explain such behavior.

Sample	E (GPa)	σ_y (MPa)	UTS (MPa)	σ_F (MPa)	EL %
H1	6.4	56.4	70.29	69.9	2.4
H2	6.8	57.7	70.2	59.6	2.1
H3	9.9	68.5	73.59	73.6	1.4
H4	11.4	65.8	83.27	57.1	1.9
H5	10.9	67.6	84.71	80	1.9
H6	10.4	67	82.37	77.5	2
Theoretical	34	288	307	276.8	14.5

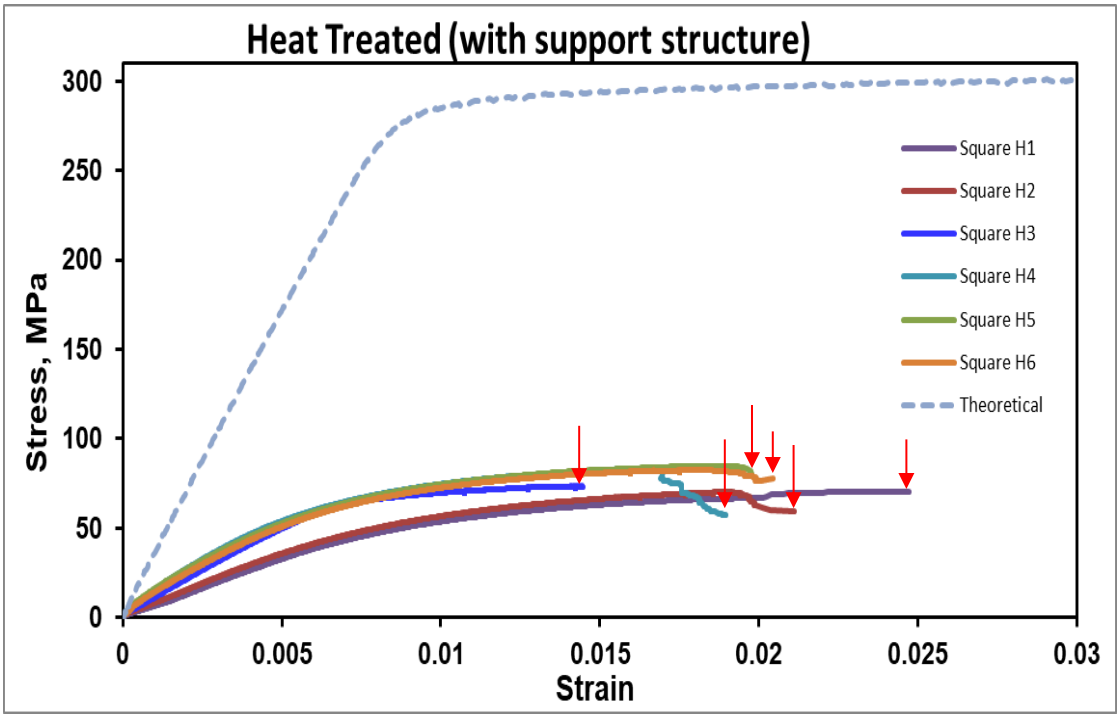

Figure 26: Stress-strain graph for heat treatment sample square base. Testing was performed by Ortho development. These samples are from the same as the non-heat-treated sample. These samples in comparison to non-heat-treated samples show approximately 3 times the tensile strength and 2 times the ductility. Heat treatment was performed without removing the support structure, resulting in a perfect build ready to test. Although heat treatment was successful, variation in ultimate tensile strength is very noticeable. In image processing, visual evidence was obtained to clarify the reason behind this variation.

Table 5: The mechanical properties of heat treated samples with support structure.

Sample	E (GPa)	σ_y (MPa)	UTS (MPa)	σ_F (MPa)	EL %
M1	8.6	65.8	72.03	67.7	1.2
M2	8.0	NA	57.35	53.7	0.8
M3	9.0	66.8	73.56	71.6	1.4
F1	8.7	NA	62.79	62.5	0.7
F2	8.3	62.5	62.95	61.6	0.9
F3	5.0	37.6	43.61	27.4	1.2
Z1	5.8	69.2	77.27	75.6	1.8
Theoretical	34	288	307	276.8	14.5

The theoretical mechanical properties that were shown in the previous tables and the theoretical graph line come from two citations. One talks about new approaches to achieve high strength powder metallurgy of Ti-64 alloy, and the other talks about modeling theoretical values for stress strain curves in composites studying deformation. See Figure 27 and Table 6. [52-53]

4.2.2 Fracture

The fracture percentage was calculated from SEM images using Image J, and the calculations used are shown in the Image Processing Section. The percentages are shown in Table 7 for each sample.

The fracture percentage shows promising results, because the increase in fracture percentage indicates an increase in tensile strength, and this result is true for all the samples. As for the over heat-treated group, the relationship stands true between the subgroups, but when compared to the whole batch, the statement needs further investigation to find the reason for the irregular result of the fracture. [54-55]

The area here has been idealized for easier fracture calculations. Specifically, the area has been calculated as if the structure is fully solid, because it is difficult to find the area of a cellular structure with 70% porosity and an even surface. Therefore, calculations are underestimated to give a sense of material behavior in comparison with each specimen. For further analysis of fracture percentage calculations, refer to the Image Processing Section.

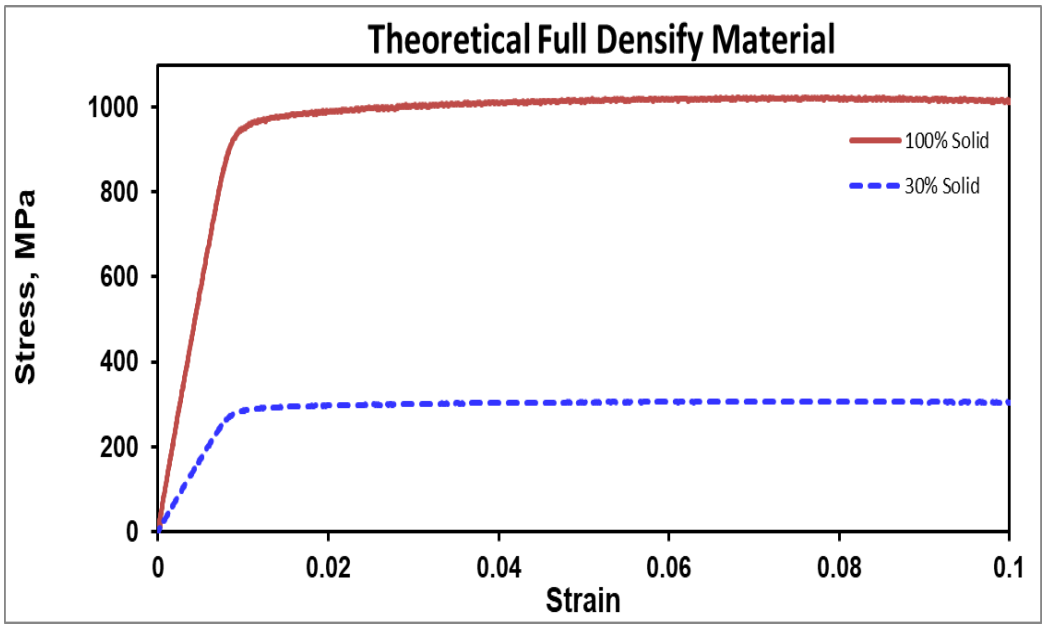

Figure 27: The theoretical data of 30 and 100 percent solid as if it was 3D printed by powder laser bed fusion.

Table 6: The mechanical properties of the theoretical values of 30 and 100 percent. The only difference in these values are the ultimate tensile strength.

Sample	E (GPa)	σ_Y (MPa)	UTS (MPa)	σ_F (MPa)	EL %
30% Solid	34	288	307	276.8	14.5
100% Solid	34	288	1023	276.8	14.5

Table 7: The fracture percentage of the specimens; S# stands for specimen number, A stands for the area, and F% stands for fracture percentage.

Non-Heat Treated			Heat treated without support structure			Heat Treated with support structure		
S#	A(mm^2)	F%	S#	A(mm^2)	F%	S#	A(mm^2)	F%
3	36.375	3.13	F1	40.39	5.7	H1	44.38	5.7
2	36.06	2.29	F2	38.82	5.2	H2	44.55	5.9
4	32.67	1.9	F3	38.7	2.7	H3	43.62	6.5
H9	42.9	3.09	M1	38.94	5.2	H4	38.28	7.7
H7	42.11	3.3	M2	38.76	5.1	H5	38.63	8.6
			M3	39.31	5.2	H6	38.89	8.3
			Z1	39.8	5.8			

4.3 Microstructure Evaluation

4.3.1 Optical Images

Microstructures can reveal details that assist the investigation. The features in Figure 28 representing the β phase and the background represents the α phase. Because the parts are additively manufactured, pores can be detected and are seen in Figure 28. In Figure 28 A, the β phase appears to be very chaotic and small compared to Figure 28 B. As for the heat-treated specimen microstructure, the β phase is very organized and grouped, showing orientation in a preferred direction as well as β phase growth. As for the α phase in Figure 28 A, it is difficult to detect the phase without segmentation; as for Figure 28 B, the α phase appears as equiaxed structures and as striped structures, and that is shown in detail in the next section. The arrangement of the α phase increases the alloy strength, and the distribution of phase increases ductility. These two results are shown through tensile testing mentioned in the Mechanical Testing Section. Heat treatment increases the alloy mechanical properties, but the treatment did not remove the pores, as shown in Figure 28 A and B. The heat treatment specimen examined was from the batch when heat treatment was a success. [56]

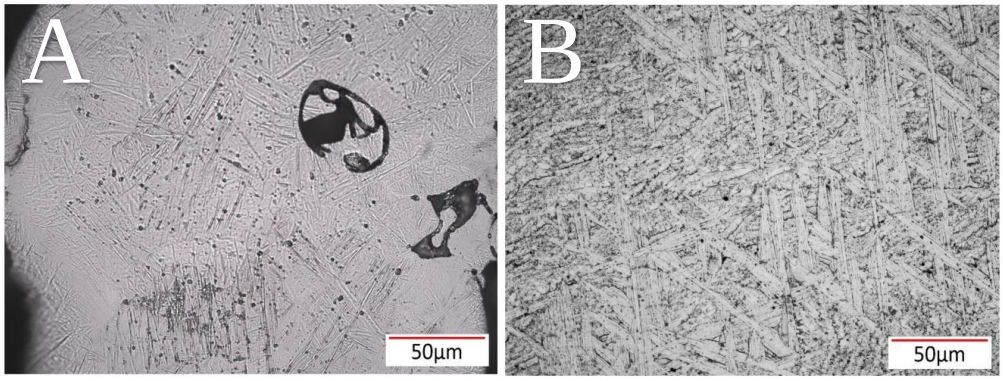

Figure 28: Optical image of Ti-64 microstructures, (A) Optical image of a non-heat-treated specimen of Ti-64. (B) Optical image of a heat-treated specimen of Ti-64.

4.3.2 Phase Identification

Figure 29 shows that the structure is a lamellar stabilizing β phase, and this phase enhances ductility. Dark lines in the figure represent the β phase, while the white sections represent the α phase. The figure also shows there are two primary shapes for the α phase, equiaxed and lamellar. The equiaxed phase is minimal, since the heat treatment was performed to target laminar phase growth. As for the lamellar phase, it consists of two phases, acicular and columnar. According to the literature review of such Ti-64 structures, the acicular phase is thin and needle-shaped, whereas the columnar phase is thicker. Other than size, both structures refer to the α phase being described as laminar. Different heat treatment targets different structures based on the application and mechanical properties that must be tested. Refer to the Future Work Under Cooling Rates Subsection for more details about heat treatments and different microstructures that can be achieved. [57]

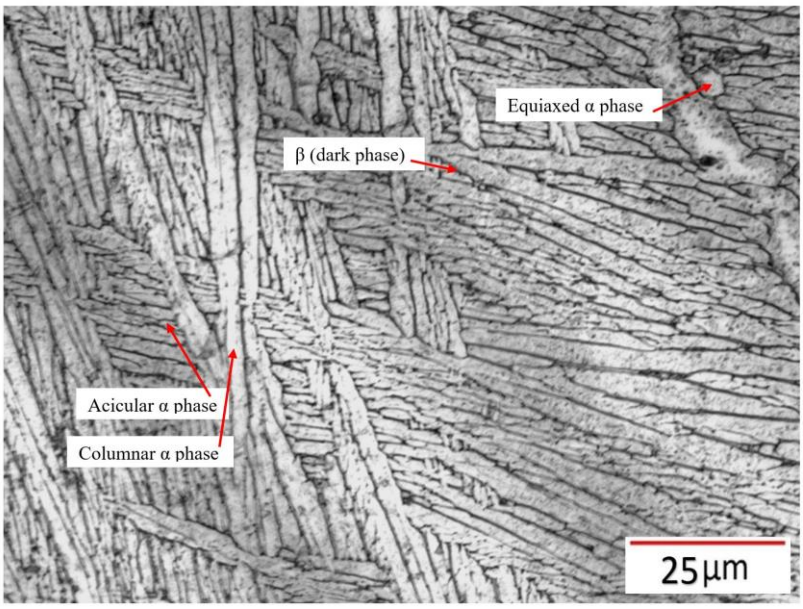

Figure 29: Heat-treated specimen microstructure of Ti-64 showing “basket-weave" or Widmanstätten microstructure.

4.3.3 Stereological Parameters

Figure 30 shows an interesting structure with different α lamellate sizes. Mechanical properties are highly affected by the orientation of colony/ α lamellate, and heat treatment and cooling rate play a major role in forming the microstructure and enhancing α or β phases to grow. For more cooling rate details, refer to the Cooling Rate Subsection. [58]

Heat treatment has been done to enhance the β phase, enhancing ductility. Refer to the TTT curve in the Future Work Section for phases transformation and possibilities for forming deferent phases to gain an understanding of the heat treatment process route.

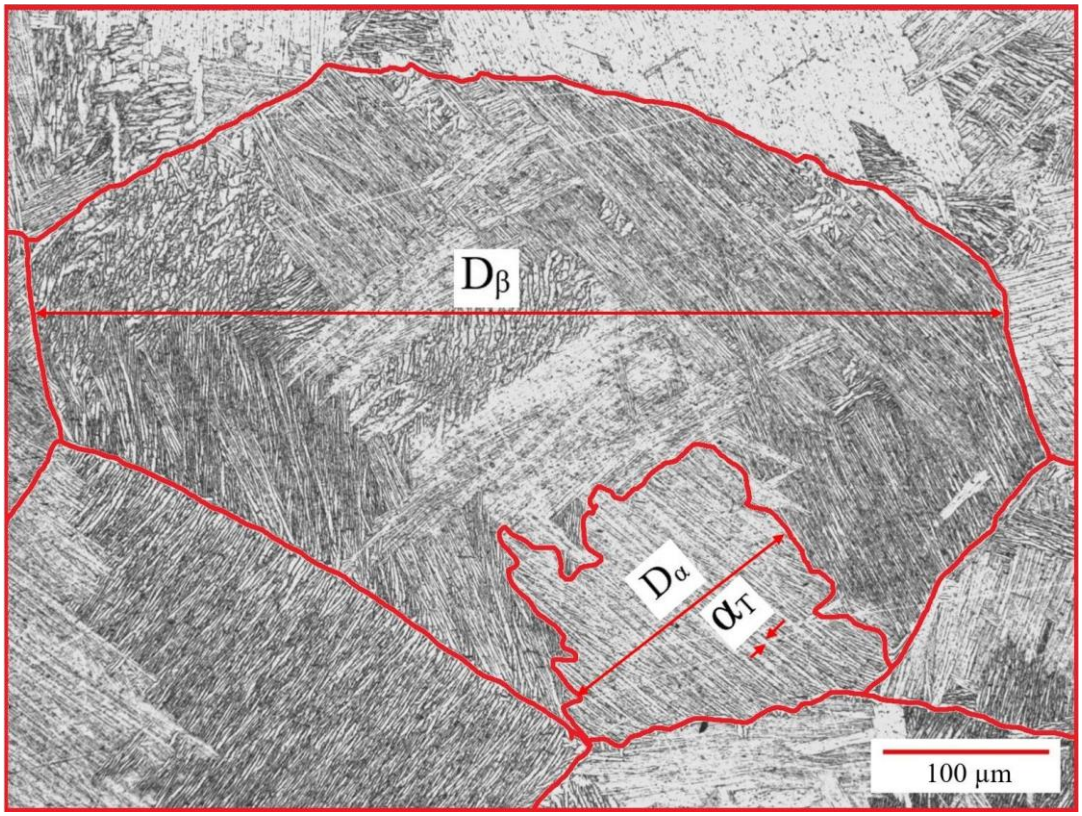

Figure 30: Optical image of a heat-treated specimen showing a lamellar structure with identifying stereological parameters. D_β represents β phase grain size, D_α represents the size of parallel α phase colony, and α_T represents the thickness of α lamella within the colony.

4.3.4 SEM Images

Figure 31 shows the effect of sintering. Without heat treatment, the powder can be seen as round particles around the main structure where powder particles became fused to the structure after sintering. The variability in mechanical properties can also be assumed to be caused by the powder particles, since the number of particles that attach to the main structure is not constant. This results in different thicknesses of the truss structure for the specimen, meaning that different tensile strengths are shown in the specimen and are observed through tensile testing data. Also, the powder has a normal distribution that influences the structure tensile strength due to the surface energy of each powder particle. The effect of surface energy becomes critical in sintering, and that is the reason for having the semi-sintered particles shown in Figure 31 A and Figure 31 B. The image has been processed to focus on a small area, making it easy to compare images. [59]

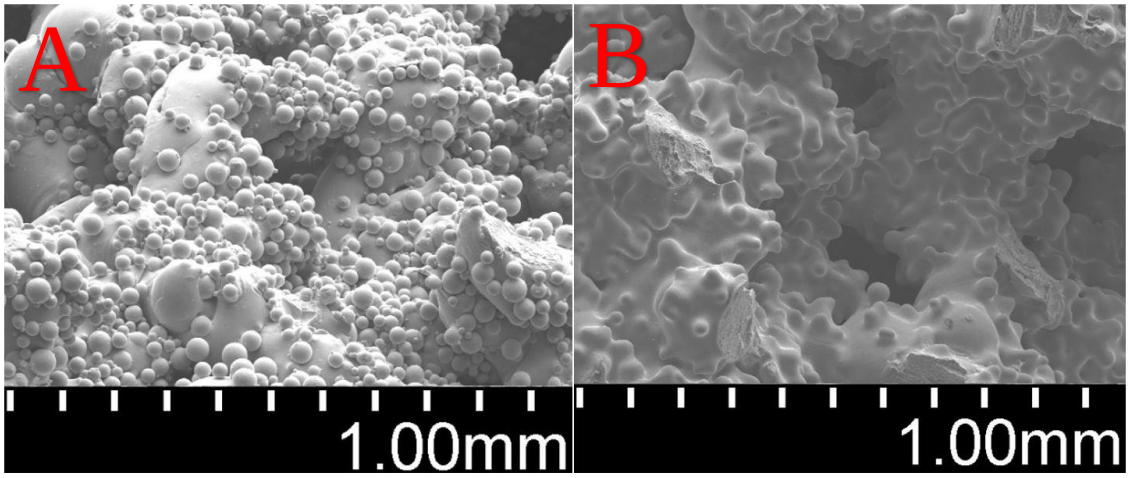

Figure 31: SEM images of Ti-64 3D printed specimens. (A) SEM image of a non-heat-treated specimen. (B) SEM image of a heat-treated specimen.

4.4 Image Processing

Ti64 (Ti-6Al-4V) is an alloy that has been developed for use in medical implants due to its compatibility with the human body. AMT has become useful in building human bone design (marrow) out of Ti64, imitating the function of the bone. My research focuses on studying the mechanical properties of Ti64 fabricated using melt-laser sintering. More specifically, microstructure images and CT scan images were analyzed through image processing using Image J. The goal of using image processing was to relate theoretical data and experimental result to quantitative data acquired from image processing. After comparing and compiling the analysis from all sources, a design model was created to enhance the investigation of the mechanical properties. [60]

Optical and SEM images were analyzed by Image J using plugins. Plugins are built-in functions that have certain applications. There are several plugins that come with Image J, and there are plugins that can be downloaded depending on the goal of the analysis.

4.4.1 Image Analysis

The process goal for SEM images is to determine the fracture percentage for Ti64 samples. Each picture consisting of pixels, and these pixels define the picture and give dimensions in X and Y axis (width and height). As a result, a total number of pixels can be acquired for the picture. Each picture has an independent value of pixels due to its original size.

It is advised to work with 8-bit image type, because this type reduces the image size and makes the program run faster. Changing the image type results in changing the

storage size of the picture but not the dimensions (width and height); consequently, the pixel type changes based on the chosen type (Table 8-pixel type column). If the image is a binary type, then the pixel stores a value of 1 or 0. If the image is a gray-scale type (8-bit), then each pixel stores a value between 0 and 255. If it is a colored image RGB type (32-bit), each pixel stores 3 values between 0 and 255 for main colors red, green, and blue. [61]

4.4.2 Fracture Analysis

To calculate fracture from an SEM image, first, the image type must be 8-bit. Then, the unnecessary part of the image must be cropped, since Image J analyzes the whole image. Afterwards, the fracture surfaces must be manually selected and have their value set to 0, which is the value for black. For easy selection and color filling, the paint application can be very helpful and a faster tool to use in this step. Beforehand, the SEM image values can be checked through a histogram to ensure that only the fracture surface has a value of 0 and no shadow or unwanted region has a value of 0. Then, the histogram is run again to obtain the number of black pixels. Lastly, the number of black pixels is divided by the total area and multiplied by 100 to determine the fracture percentage.

Table 8: Illustrates image depth for a pixel.

Pixel Type	Bits	Range	Description
Binary	1	0–1	Black & White
Gray Scale	8	0–255	Scale from white to black
RGB	32	0–255 for each color	Range of three colors (Red, Green, Blue) Colored image

4.4.3 Fracture Calculation Example

Step 1: Crop the unwanted part of the image, as shown in Figure 32.

Step 2: After cropping check for black color value occurrence, the value should be 0. If not, adjust brightness, as shown in Figure 33.

Step 3: Select all fractured areas and set their value to 0 (black color) or use the paint application to color all fractured surfaces black, as shown in Figure 34.

Final Step: Check the histogram of the previous image (step 3) and divide the number of black color pixels by the number of total pixels to obtain the percentage of black pixels (fracture area), as shown in Figure 35.

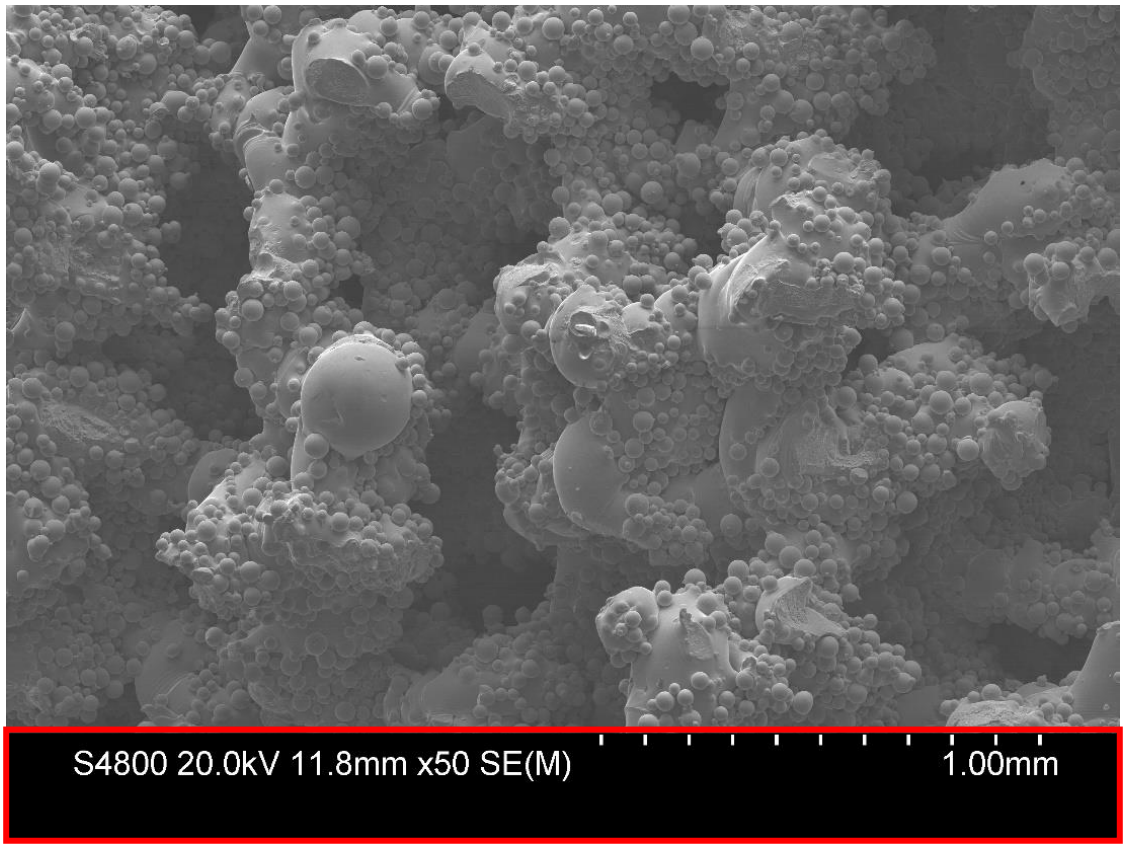

Figure 32: SEM image, unwanted part in red box.

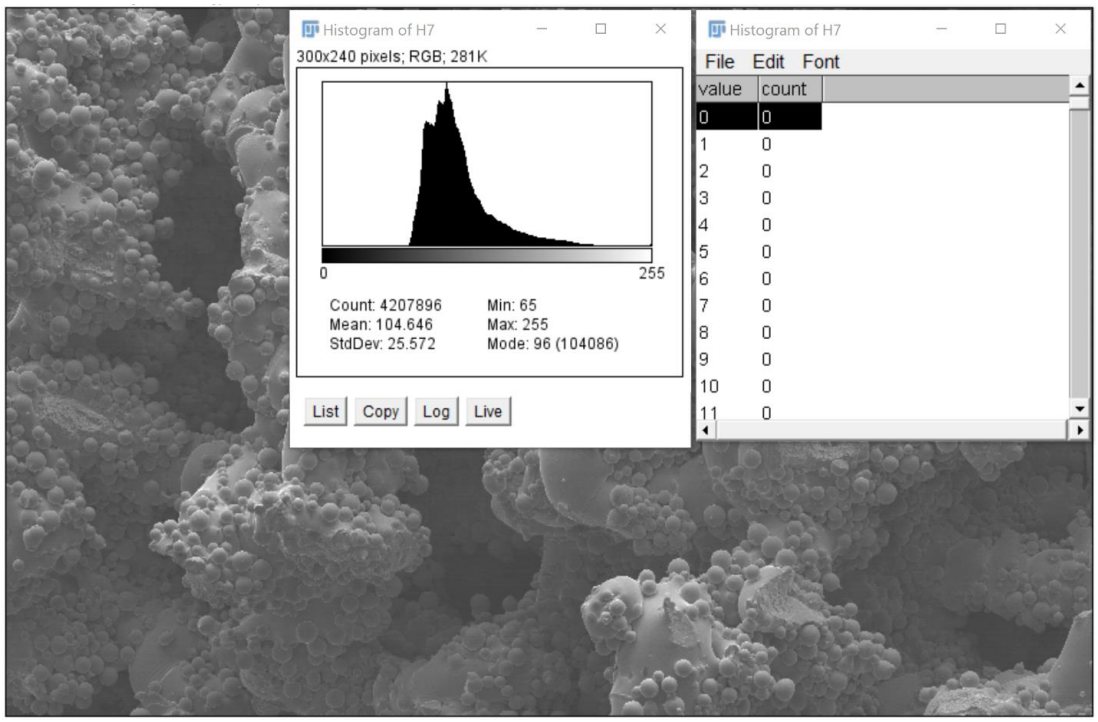

Figure 33: Checking for black color value = 0, count 0.

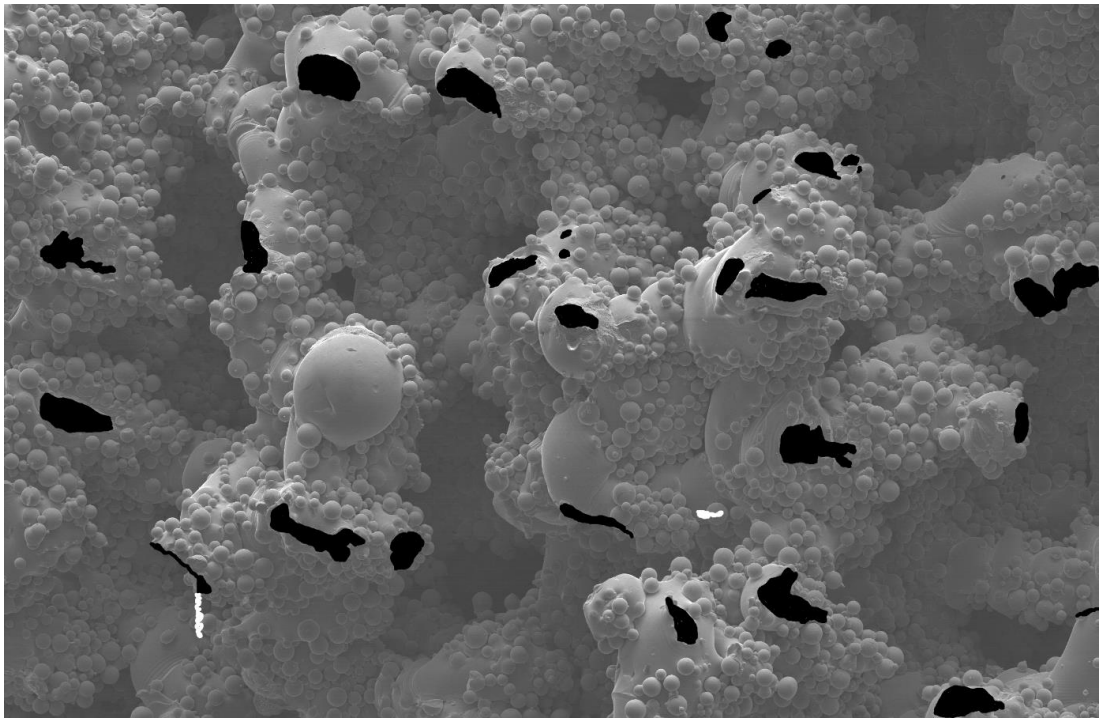

Figure 34: Selected area of interest (black); if a mistake was made, it was colored white, since it has a value of 255. White color does not change anything critical, since black pixels are the most important feature.

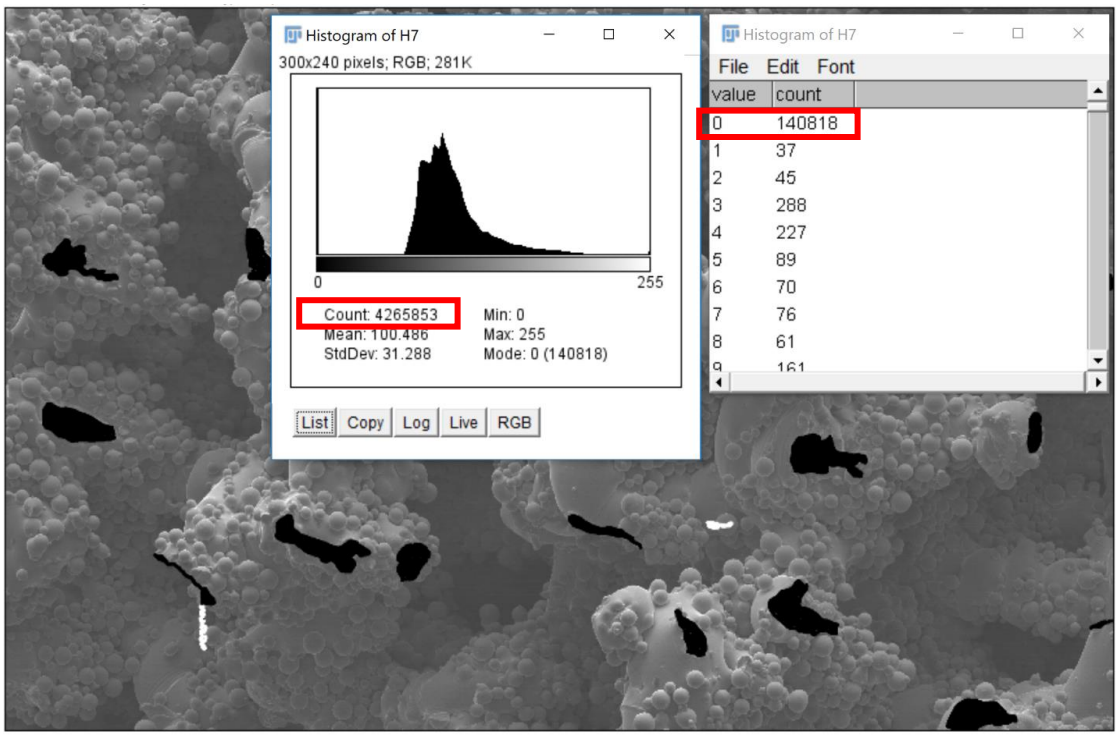

Figure 35: Number of pixels needed for calculation in red boxes.

$$\text{Fracture \%} = \frac{140818\ pixels}{4265853\ pixels} * 100$$

Fracture= 3.3%

4.4.4 Segmentation (Trainable WEKA)

Regarding optical images, the goal is to make the microstructure features visible and easy to distinguish for any grain boundaries or phases in the image. The process can help visualize multiphases, grain boundaries, voids, and whiskers. There are several plugins that can be helpful in analyzing optical images due to the goal desired such as skeleton, segmentation, and volume viewer for CT scans. By using the segmentation plugin and then selecting the trainable WEKA segmentation, images presented in Figure 36 are produced to provide better visual analysis.

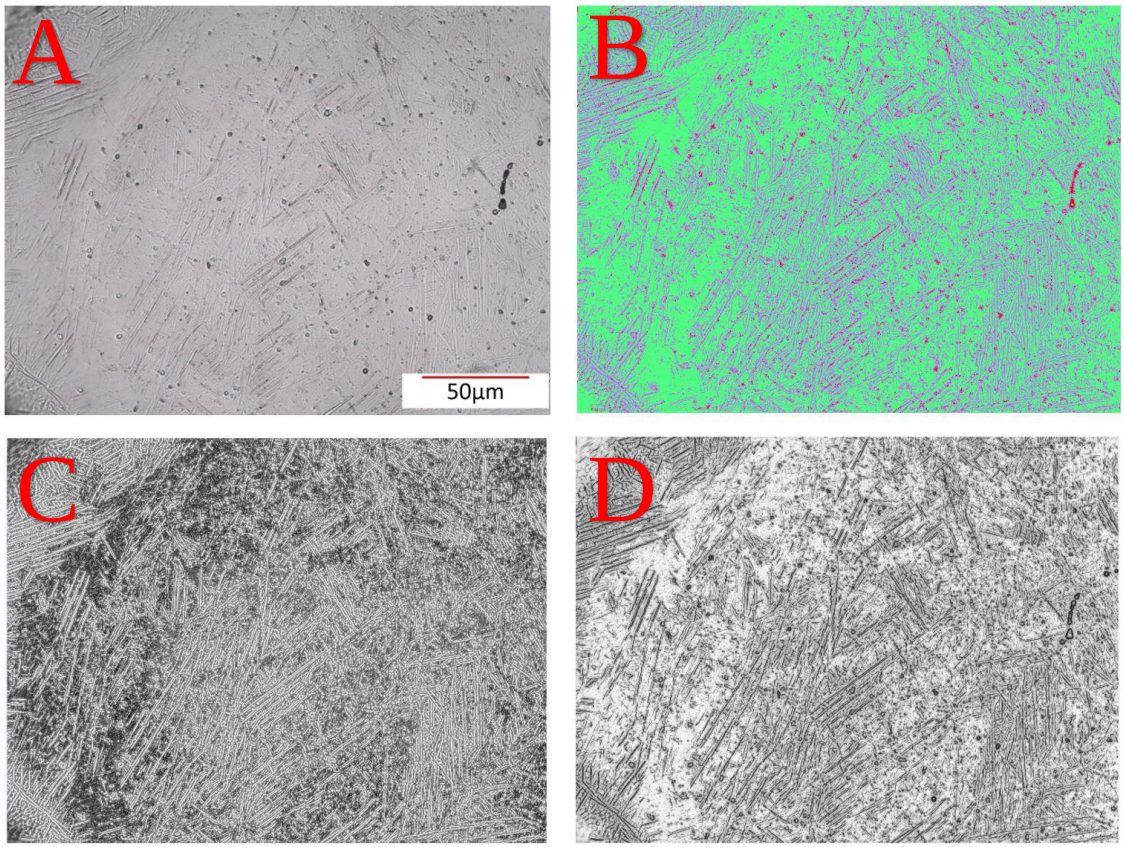

Figures 36: Image processing of Ti-64 microstructure. (A) The original image. (B–D) Image processing stages of image (A) using the segmentation WEKA plugin.

Figure 36 A shows the original optical image, and it has the scale on the right bottom corner of it. The scale is the same for the other images, but it has been removed for easier processing and inspection. Figure 36 B was created according to three classes. The first-class background is shown in green, the second-class background is the feature of the microstructure of Ti-64 and is shown in purple, and the third-class background comprises the pores shown in red. Figure 36 C highlights the feature of the microstructure. Lastly, Figure 36 D highlights the background.

After performing the steps in Figure 36, further analysis can be performed to calculate the normal distribution of pores and sizes of them by using the detect circle

plugin. In this research, it is not a priority to do such analysis, but it can be done as a part of future research work.

One of the most useful tools used for this research is the segmentation plugin. Segmentation uses several other plugins to detect features that are selected manually. For example, it can detect edges, circles, and all irregular shapes by color value. There are separate plugins that can do individual segmentation such as detect edges and circles. Detect edges plugin is a fast way to identify edges only. Similarly, detect circles works in a similar manner as detect edges, but it only identifies circles. Segmentation WEKA plugin does a great job at detecting, combining all techniques to provide the best segmentation, but it takes a bit longer than other plugins, producing greater results. Selecting more segmentation lines yields better evaluation and a better segmentation result. The images that are produced from segmentation WEKA are classified according to their classes that were chosen by the user. Each image provides information about a class by highlighting it to make it clear and easy to see. [62]

4.4.5 Wall Thickness

The wall thickness can be determined by using two plugins: distance map and skeleton. Distance map is a plugin that relates an object and another by giving several gradual values to identify the distance between the two objects. Skeleton is a plugin that simplifies all the image features to simple lines. Similar to a human skeleton, it is a good analogy to make easy understanding of distance map and skeleton plugins. The distance map is simply the human flesh, and skeleton plugin is the human skeleton in the simplest form as a human stick figure.

The addition of the two images from distance map and skeleton provides a unit cell net that surrounds all features. That simple calculation can be performed to determine the wall thickness of the Ti-64 features in Figures 37 and 38. [63]

Figure 38 A shows the basic mapping of Figure 37, and Figure 38 B also shows a basic mapping of Figure 37 but with a gray-scale. These two figures add together, showing wall thickness using a coloring code on a green-blue scale. Finally, the wall thickness image is added to the original image in binary formatting, giving the full wall thickness mapping of Figures 39 and 40.

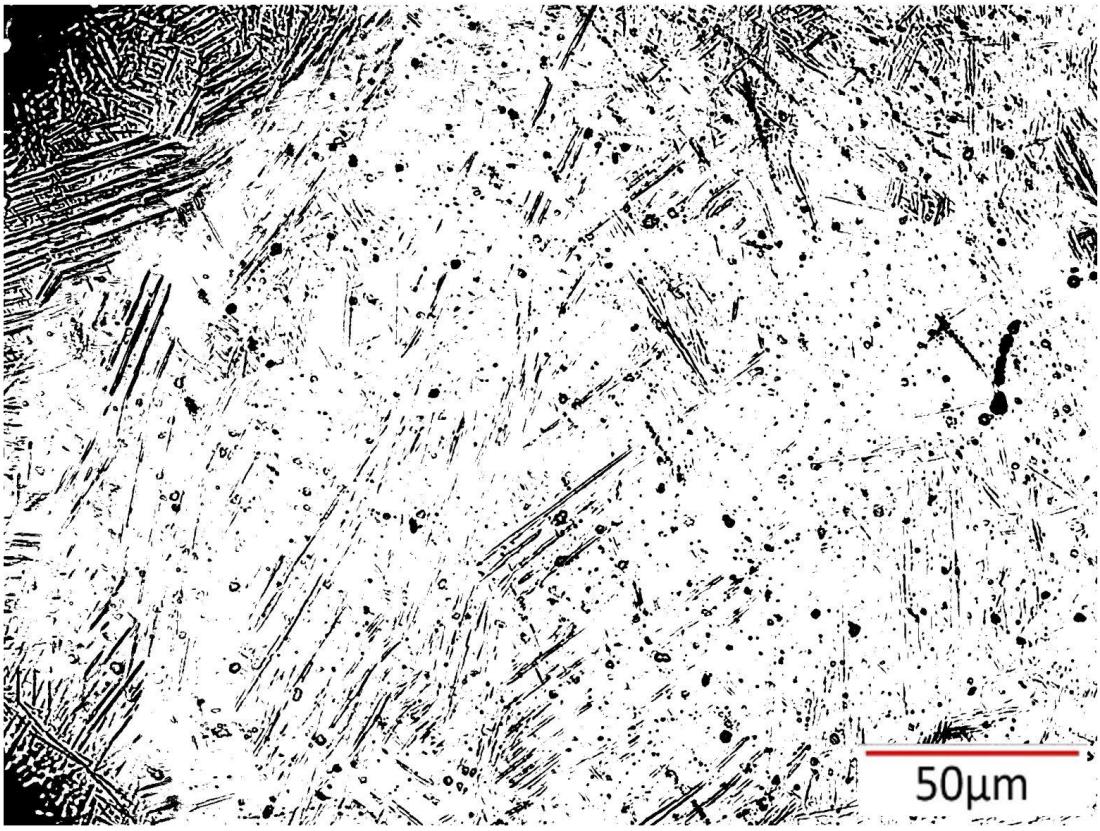

Figure 37: A binary image of the original image, Figure 36. The binary process transforms an image to black and white, reducing the size of the picture so it is fast to process and manageable to store.

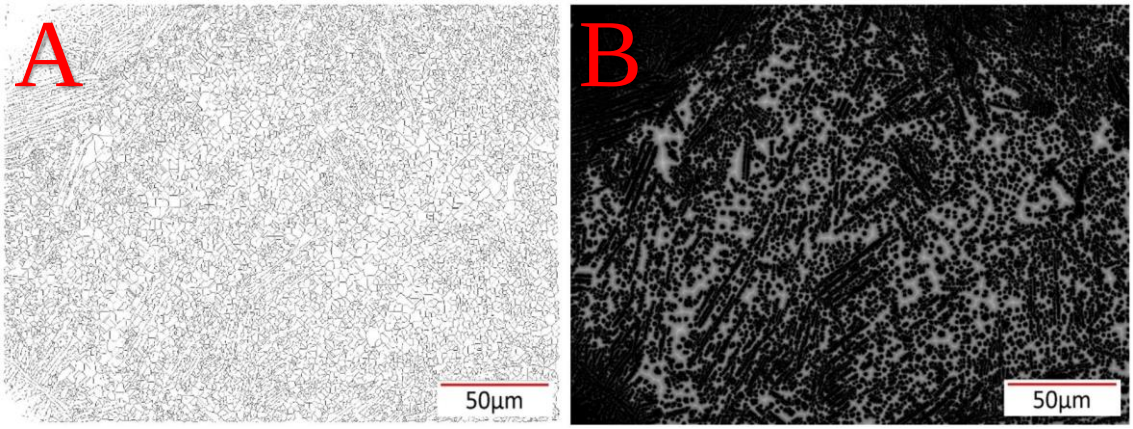

Figure 38: Image processed using skeleton plugin and distance map function. (A) skeleton map of Figure 37. (B) distance map of Figure 37.

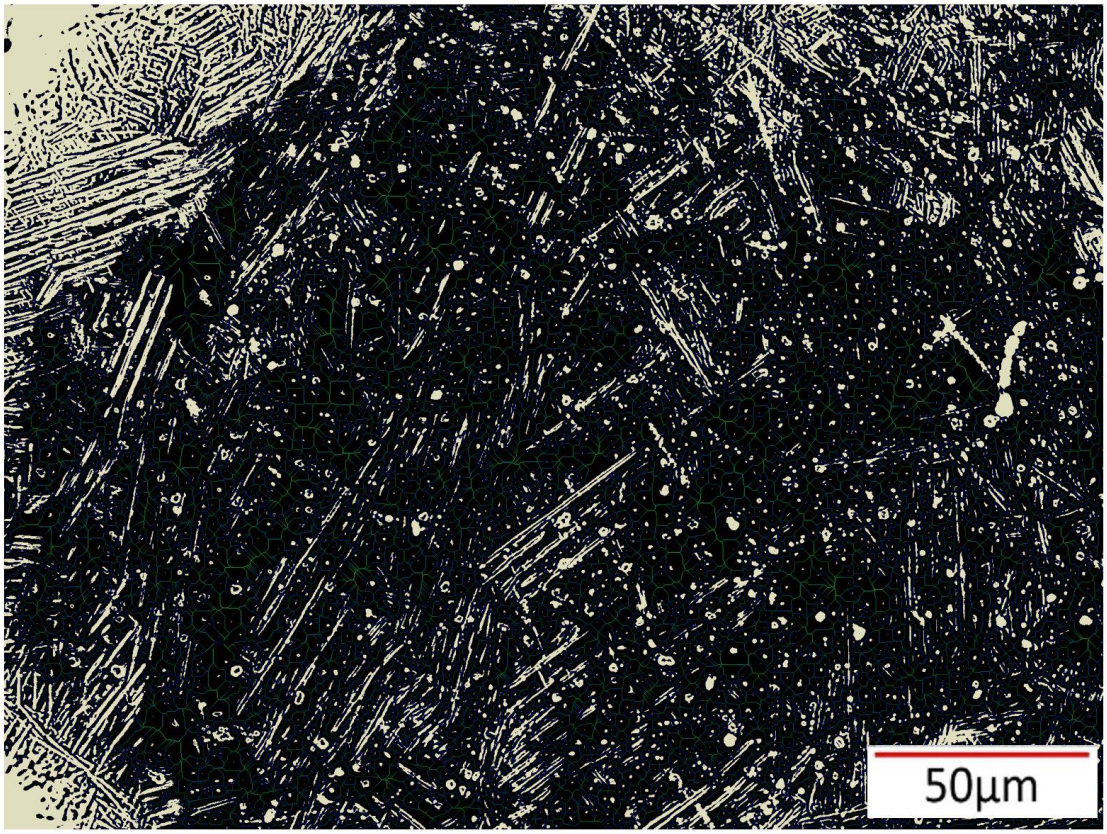

Figure 39: An image of wall thickness mapping combined with the original image in binary form.

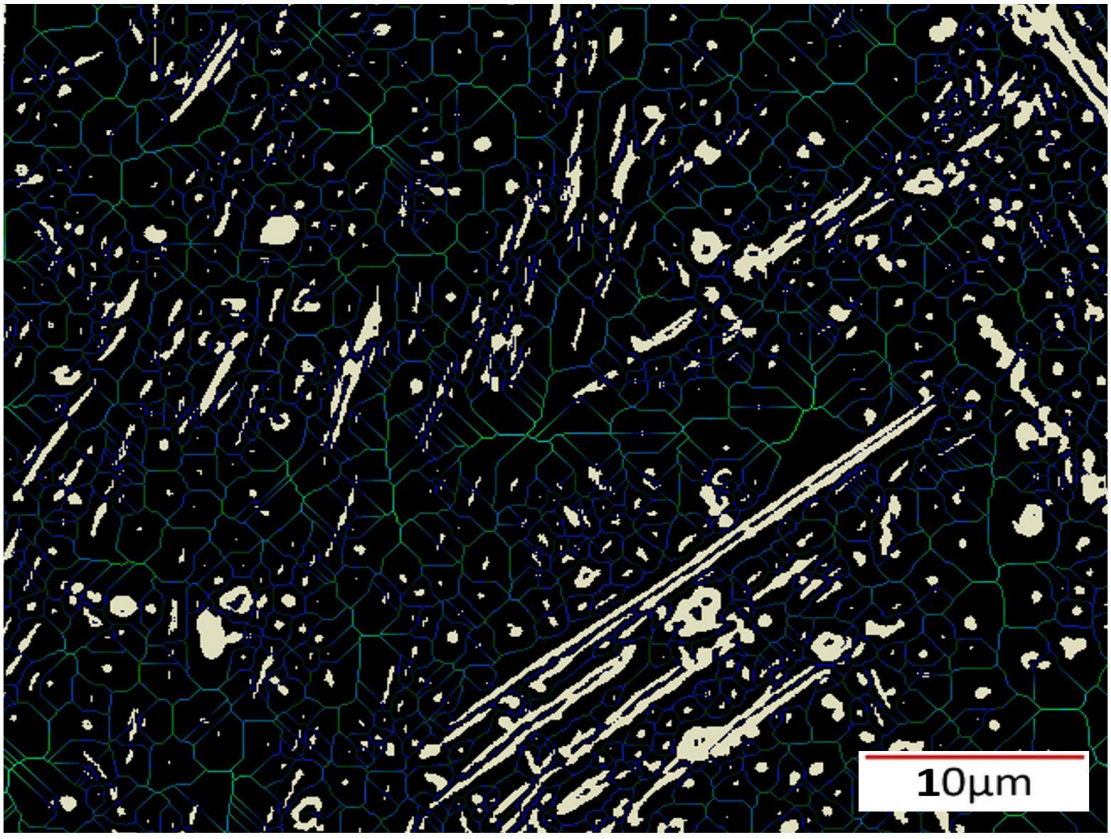

Figure 40: A close-up image of Figure 39, showing wall thickness of features in (white). The light color (light green) represents a wall thicker than the wall represented by the dark color (dark blue).

Wall thickness can be calculated by taking the value of the wall "green-blue veins" and multiplying the value by 2 to give the diameter value of the wall in pixels. Knowing the magnification on the image gives the final answer of wall thickness in micrometers. Similar calculations are presented on 3D modeling in the next section. In addition, the values of the wall color can be acquired by viewing the histogram of the image. For more information on histograms, refer to the previous section where fracture percentage was calculated.

4.4.6 3D Modeling

Figure 41 A shows a 3D image of the cellular structure that was built to be tested mechanically. CT scanner builds the image by slicing the sample and building a 3D model. By applying the wall thickness process that has been introduced earlier, Figure 40 B is produced. Figure 41 B shows a representation of the inner cellular structure. The inner cellular structure image shows nonuniform powder melting agglomeration in the red circle. There are several of these agglomerations across the build. This phenomenon happens randomly due to the Ti-64 powder properties, and it can vary the mechanical properties of the cellular structure.

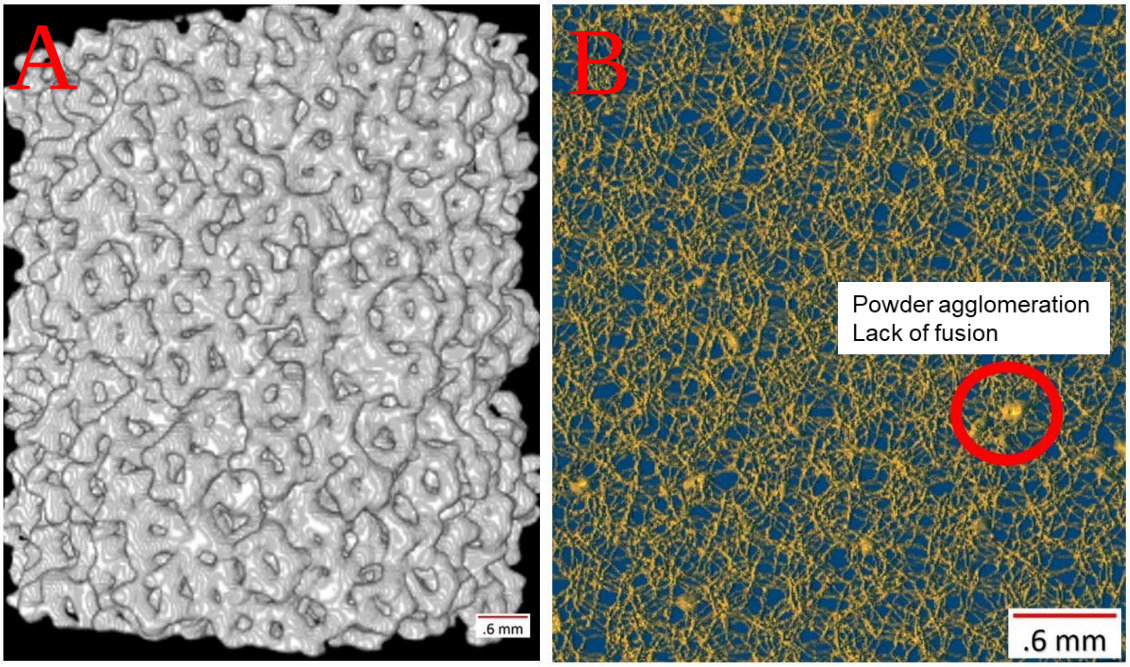

Figure 41: CT scan of Ti-64 section of gauge length of the specimen. (A) CT Mapping and 3D image of Ti-64. The diameter of 6.86 mm and height of 6.68 mm. (B) Wall thickness of 3D image in (A). Sign of agglomeration in the red circle.

4.4.7 Unit Cell Parameters

Furthermore, analysis has been performed to calculate the unite cell diameter (one Tetradecahedron structure). The diameter was calculated by dividing the diameter of the cellular structure by image pixels and then multiplying the result by the calculated diameter of the unit cell in pixels, giving the diameter of the unit cell in millimeters. The diameter of the cellular structure is 6.86 mm, there are 400 image pixels, and the unit cell diameter calculated from the image is 35 pixels. The calculated diameter of the unit cell is 0.60025 mm, and the programmed diameter of the unit cell is 0.7 mm.

$$Diameter\ of\ unite\ cell\ (mm) = \frac{6.86\ mm}{400\ pixels} \times 35\ pixels = \ .60025\ mm$$

Figure 42 shows a normal distribution of a thickness of all the cellular structure that has been scanned. Pixel values have been converted to be in about 0.2004 mm as an average value. The graph in Figure 42 describes the wall thickness of the cellular structure, and the high values start from 0.25 on the graph. The high values are the agglomeration that has been described previously in the skeleton graph. The calculation of cell membrane (wall thickness) is as follows.

An example:

$$Wall\ thickness\ of\ the\ trusses\ (mm) = \frac{6.68\ mm}{400\ pixels} \times 2 \times 6\ pixels = \ .2004\ mm$$

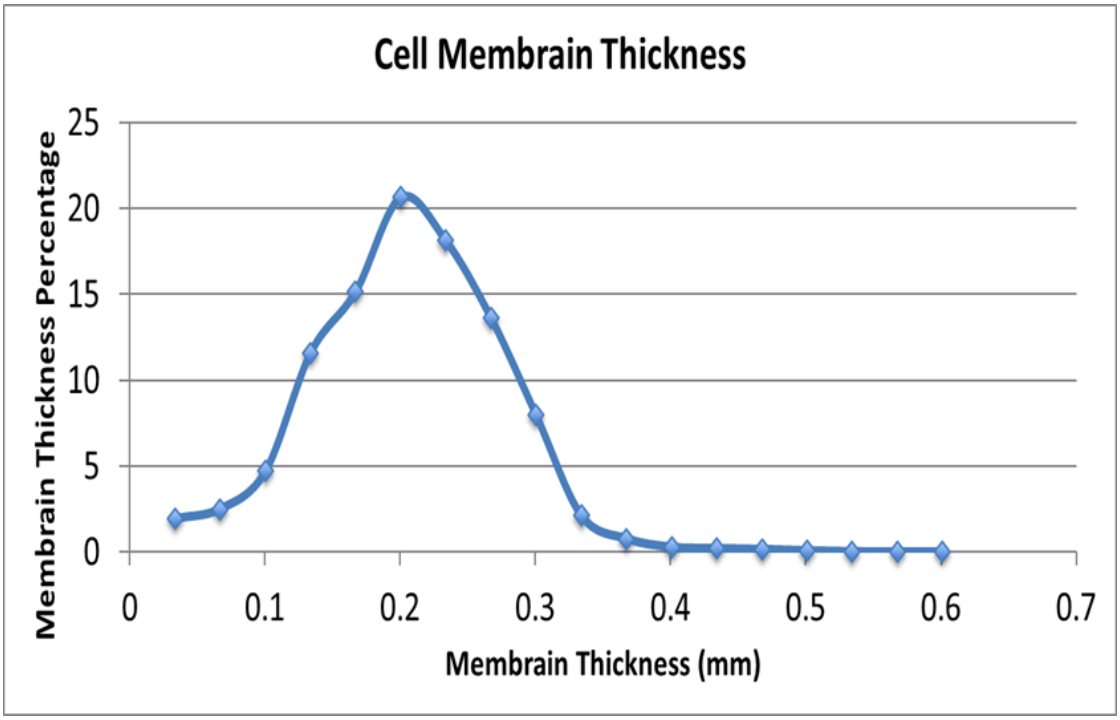

Figure 42: Cell membrane (Wall thickness) counts for the 3D CT Figure 41 A).

4.4.8 Powder Agglomeration Mechanics

As presented in the previous section, the structure has a normal distribution wall thicknesses. The reason being is that when the truss of a Tetradecahedron structure is printed, the powder particles around the main build get randomly attached to the truss. These attached powder particles add an amount of wall thickness to the truss structure. In addition, agglomerations of powders are shown at some points, and these are most likely the corner of a Tetradecahedron where several trusses meet. Figures 43–46 show the top and side views of this mechanism, giving an approximate visual evidence for this phenomenon. Figure 43 shows a schematic of a Tetradecahedron truss surface, showing random powder particles attached to the truss (in green). After sintering, depending on the particle size and contact angle, powder particles show the different shapes and bumpy

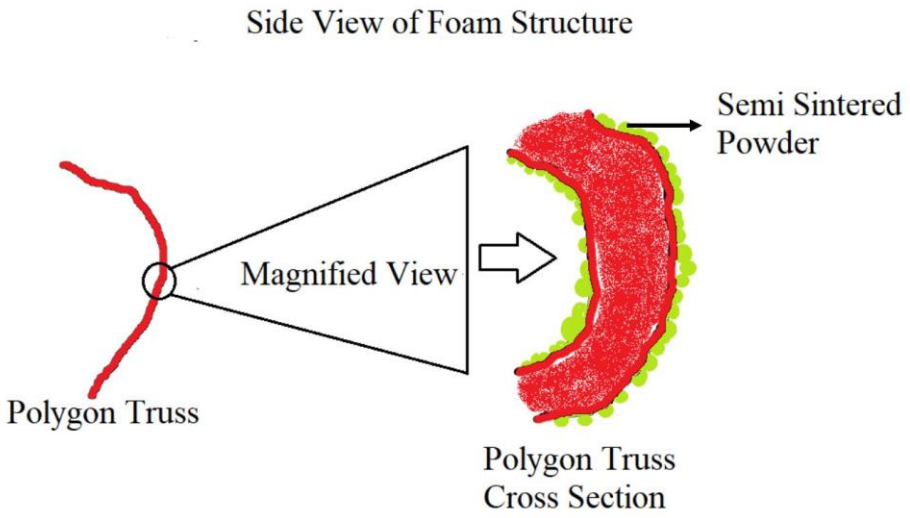

Figure 43: A schematic of a Tetradecahedron truss segment surface showing random powder particles attached to the truss (in green).

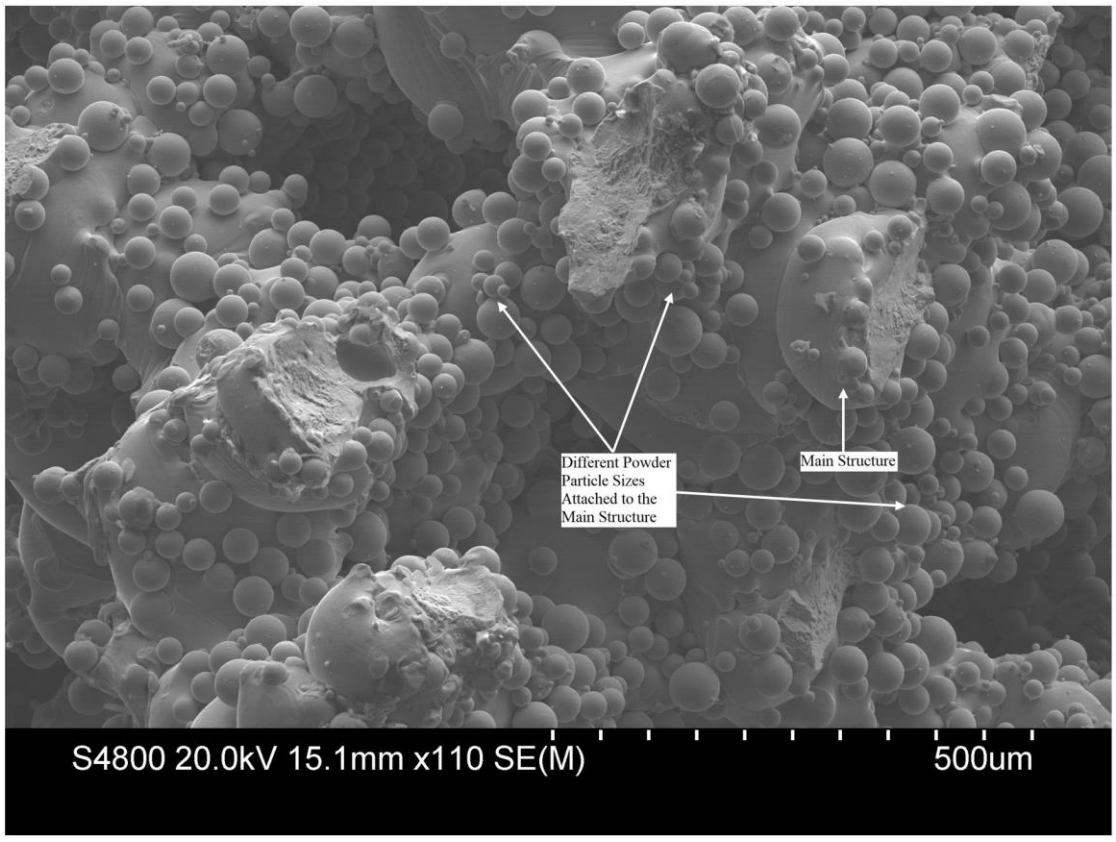

Figure 44: SEM image of low magnification showing the main structure and the powder particles that have attached to the main structure of the heat-treated sample.

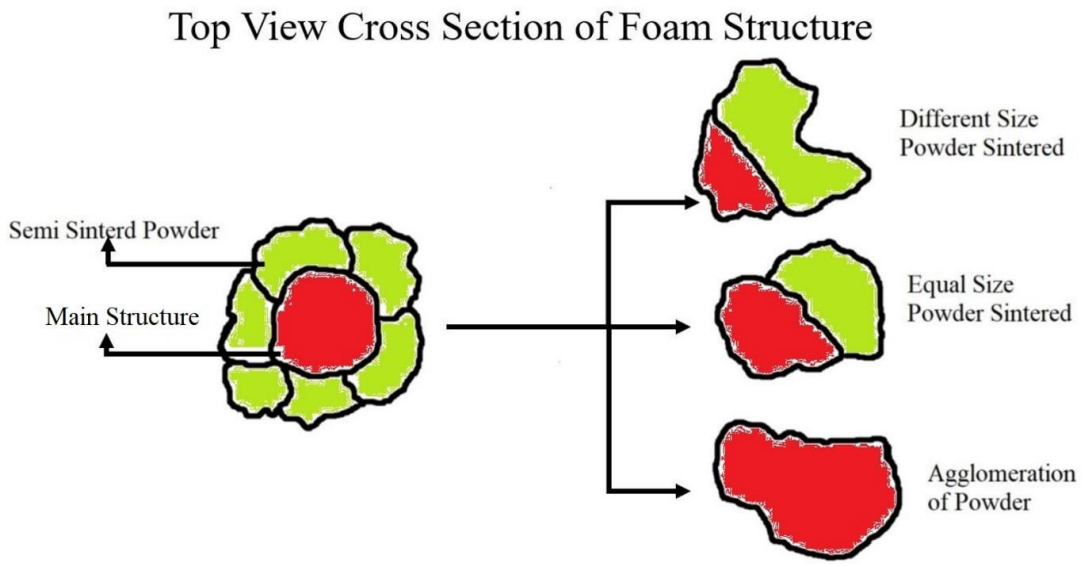

Figure 45: Schematic of the attachment of powder particles to the main build from the top. On the right is the mode of sintering that the powder falls into. The first case is when the attached powder is larger than the main structure relative to surface contact and due to poor surface contact, leading to poor sintering. The attached powders appear as protrusions in SEM images or semi-spheres attached to the main structure after sintering. The second case is when the attached powder has the same size as the main structure, and the attached powder appears as a bumpy surface. The last case is when the powder particle becomes part of the main structure after sintering, causing locally thickened points that can be observed through a CT scan (refer to Figure 41).

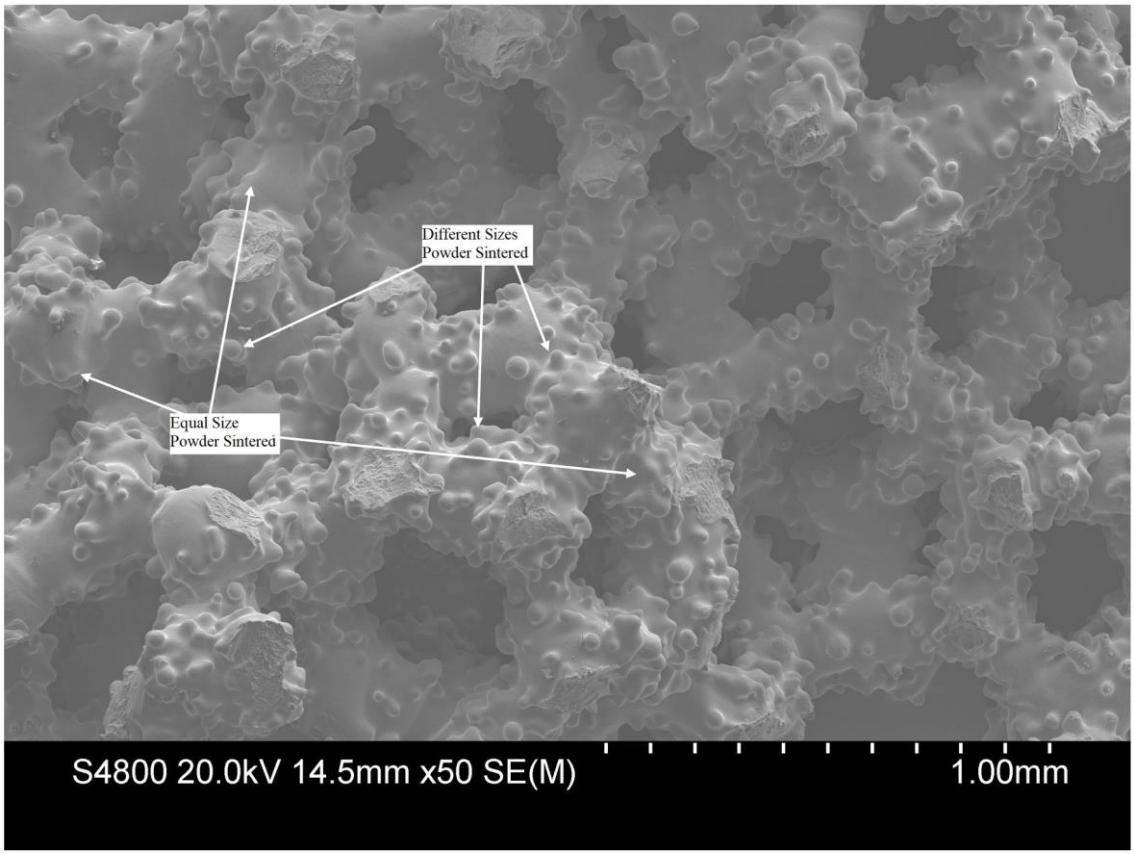

Figure 46: SEM image of the heat-treated sample with low magnification.

surface sizes that are critical to this structure, since Tetradecahedron size is in micro scale. If the structure is large enough relative to powder size, then this issue becomes negligible, but such an assumption cannot be made since it defeats the purpose of this research. Figure 44 shows an SEM image of low magnification, showing the main structure and the powder particles that have attached to the main structure of the heat-treated sample. Figure 43 shows what can be observed from this SEM image in the simplest manner. As stated previously, the powder particles attach in a random manner, meaning there is no way to make identical Tetradecahedron structures with identical wall thicknesses using this process. The build is on the micron level, and the attachment of powder particles affects its mechanical properties. This effect is shown in the tensile

testing graph where variability in specimen strength can be observed, and the powder attachment phenomenon is one of the reasons for this variability in mechanical properties. [64] In addition, Figure 46 shows an SEM image of the heat-treated sample with low magnification. As discussed in the schematic in Figure 45, Figure 46 shows that different sized powder particles after heat treatment appear as protrusions on the surface. Equally sized powder particles sintered appear as small bumps on the surface. The agglomeration of powder is easier to identify in CT scan images processed, as shown in Figure 41. Although heat treatment was effective, as presented in the improved tensile test yield strength, Figure 46 shows that some powder particles maintained their semispheric shape. [65]

CHAPTER 5

FUTURE WORK

5.1 Poisson's Ratio

Poisson's ratio is a great indicator of the mechanical behavior property. From it, deformation of the material under load can be determined due to tension or shear stress. Poisson's ratio is the lateral contraction strain divided by the longitudinal extension strain in the specimen tested, and the value of Poisson's is between -1 to 0.5 for materials. A positive Poisson's ratio means the width of a specimen decreases in width when tensile loads are applied to the specimen until failure, and that process is very straightforward. In contrast, a negative Poisson's ratio means that the specimen expands or twists when a load is applied. Metals cannot do such a thing unless a composite is made using them, and these composites are fabricated by making different orientations of the layers by placing them at angles. Consequently, while the specimen is in tension, some of the load converts to shearing stress, and the specimen fails in a sheer mode instead of a tensile mode. As a result, the structure of the composite controls the manner that the material/alloy fails, so it can protect against a type of failure based on the application, possibly protecting the user from getting seriously injured. An example of that would-be car accidents; instead of the components of the car in an accident breaking toward the

driver, they could break instead away from him, increasing safety. [66-68]

5.2 Cooling Rate

Cooling rates play a major role in forming phases and controlling microstructure formation. Therefore, experimental data about different cooling rates for Ti-64 cellular structure are important and essential to control mechanical properties and enhance them, as the application specified. Such a study has been made for solid Ti-64 through different processes other than AM. Figures 47 and 48 are from the study conducted by the Dr. Fang group at the University of Utah Metallurgical Engineering Department showing that different cooling rates and heating profiles may form different microstructures. [69]

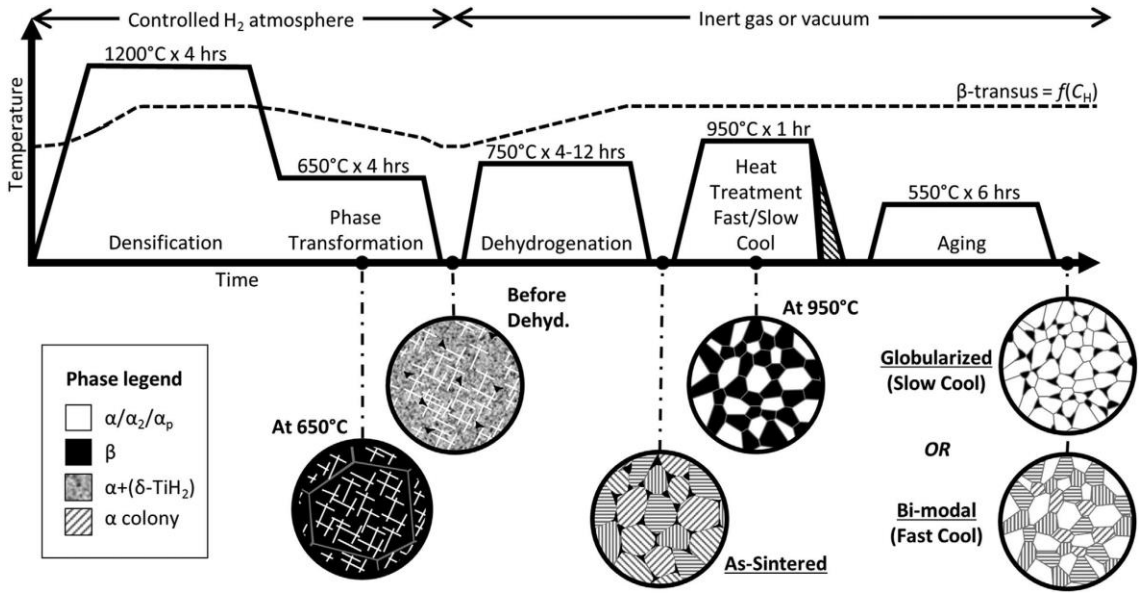

Figure 47: Schematic of the thermal profile, microstructural evolution, and the β-transus (as a function of hydrogen content) during hydrogen sintering and phase transformation (HSPT) and subsequent heat treatments to produce Ti-6Al-4V with bi-modal and globularized microstructures. [70]

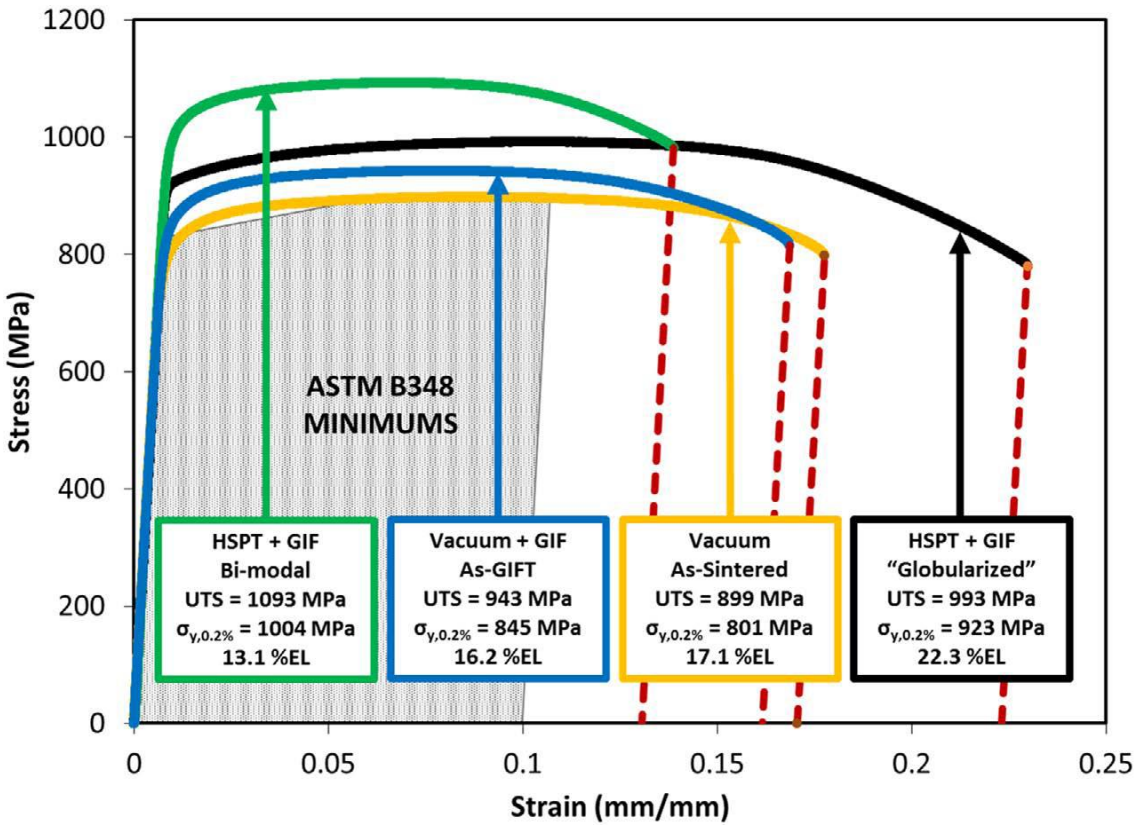

Figure 48: Tensile stress-strain curves for Ti-6Al-4V produced via HSPT and gaseous isostatic forging (GIF) with subsequent heat treatment to produce bi-modal and globularized microstructures, as well as conventional vacuum sintering with and without GIF. [71]

The idea is that following the same example by producing different stress-strain curves for the AM Ti-64 cellular structure fabricated with different cooling rates and different process production routes helps show the various mechanical properties, such as shown in Figure 48, and the materials used in various applications may be determined based on the requirements of the materials in the applications. Also, it is beneficial to model the heat profile for Ti-64 cellular structure, as shown in Figure 47. Lastly, researching the possibilities of structural enhancement, and subsequent mechanical property improvement, by studying the effect of cooling rates can be the next step of this

research.

5.3 Ti-64 (TTT) Curve

The temperature, time, and transformation (TTT) curve is the key to fabricating the alloy with precise mechanical properties by following a pattern shown on Figure 49 to avoid creating unwanted phases. The easiest TTT curve to understand is the iron phase diagram, and reviewing it provides a solid understanding of these type of curves. As mentioned, the heat treatment was performed for creating α+β phases by holding the temperature at 1300°C for 8–10 hours. There are other possibilities and ways to also enhance the phases. For example, oscillating in a small temperature difference creates equiaxed phases such as spheroidized steel. [72]

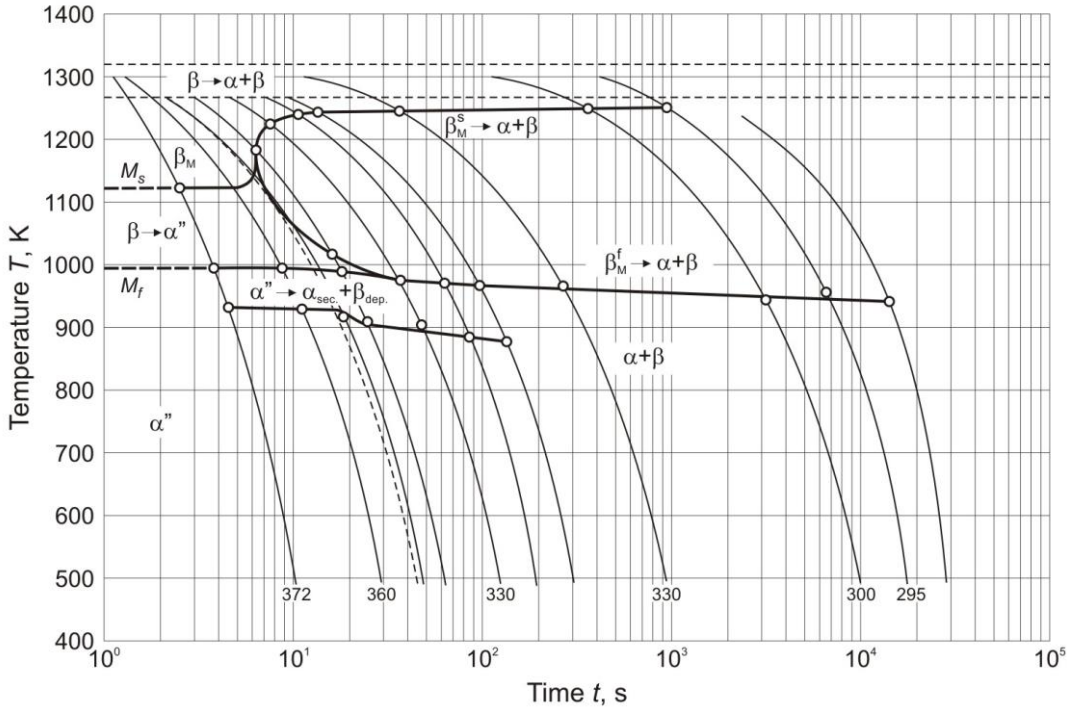

Figure 49: TTT curve of Ti-64. Phases can be shifted to the right by adding stabilizers to make the phases transformation easier to achieve. [58]

5.4 (XRD)

X-Ray diffraction (XRD) can be used to determine the plane-orientation percentages of each phase in the printed Ti-64 alloy that has been printed. Also, the reverse pole figure can be obtained to show the Ti-64 texture. Controlling the texture can enhance mechanical properties, and it can target a specific direction of strengthening (x-y directions), making the material show high strain resistance in one direction and low strain resistance in the other. The strengthening is proportional to the x-y direction, because it is just an arrangement of crystals, making them grow in a certain direction. XRD sample preparation is sensitive, because the sample needs to be flat with a mirror finished surface, preferably a non-etched surface. Variation of errors can occur with different indicators such as a peak width being wide, the peak intensities occurring on shifted angles, a large amount of noise data and possible double false peaks due to the surface roughness. Therefore, the sample must be mirror polished well for accurate results.

There are other good ideas that can be applied to this research, and this research will hopefully be resumed and produce more results by focusing on the control of phases based on the presented ideas.

CHAPTER 6

CONCLUSION

Overall, developing a new process and structures requires good research. This paper gives an overview of things that must be considered while manufacturing cellular structure for applications. The information has been presented so other researchers can learn from it and apply it to their own design to solve process challenges.

Tensile testing is one of the most important tests due to its effectiveness in terms of data analysis and being cost-effective. The tensile test gave information about strength and ductility and showed variation in the batch that was tested. Consequently, heat treatment was necessary to attempt to reduce the mechanical properties variation, but that did not solve the challenge. Therefore, a CT scan was necessary to internally analyze the structure and determine and analyze any evidence of variability.

Sintering is a very important concept to understand to strengthen parts made by another technique, as the case study showed. In powder preparation, packing of the powder in the dye (before pressing) was crucial to obtaining a strong green part with uniform green density, because failure to do this step led to green part failure in some cases. Sintering of fine powder parts was more successful than coarse powder parts, which was expected. This is because of the higher surface energy (higher driving force of

the finer particles). For example, changing the temperature from 1100°C to 1200°C showed significant improvement in densification of fine powder parts, but little change for coarse powder parts. The best results were obtained when sintering fine powder parts at a higher temperature of 1200°C.

Image J is a powerful tool that can compile the analysis to enhance results and save time for other operations such as SEM imaging and EDX. It has various tools to choose from to aid in analyzing optical images of Ti-64. By analyzing the basic optical images, time and effort can be minimized by knowing exactly which regions to target for SEM imaging and to detect elemental percentage by EDX. Image J also can enhance images in many different ways to give the optimum result needed for quantitative analysis or qualitative analysis depending on the research objective. Changing image type to 8-bits is important so that it easy and fast to run. Also, Image J saves a lot of data, since storage on computers is very limited. Also, Image J can analyze 3D images that are produced from CT scans, and the results can be saved afterward as an STL file so 3D printers can reproduce the scanned shape. A 3D image is basically many 2D-image slices that are compiled to give volume, making a 3D image. There are many great plugins, masks, and tools to choose from to give the analyzed image the maximum potential information capacity.

Lastly, each test was essential to this research, and each chapter explains the knowledge needed to gain a good understanding of the research. The main objective is to investigate the cause of mechanical property variability for additive manufactured parts. Throughout the research, it has been hypothesized and proven that the variability comes from the AM technology used. Also, the variability comes from the powder mechanics.

These two reasons are the main reasons, but there are other reasons that contribute to mechanical variability, such as heat treatment and cooling rate, where different phases and microstructures can be produced based on the heat treatment and cooling rate.

REFERENCES

1- Spierings, A.B., Herres, N., and Levy, G., "Influence of the particle size distribution on surface quality and mechanical properties in AM steel parts," *Rapid Prototyping Journal* 17.3, 195-202, 2011

2- Wadley, H.N.G., Fleck, N.A., Evans, A.G., "Fabrication and structural performance of periodic cellular metal sandwich structures," *Composites Science and Technology*, 63, 2331-2343, 2003.

3- Moongkhamklang, P, Deshpande, V.S., Wadley, H.N.G., "The compressive and shear response of titanium matrix composite lattice structures," *Acta Materialia*, 58, 2822-2835, 2010.

4- Spierings, A.B., and Levy, G., "Comparison of density of stainless steel 316L parts produced with selective laser melting using different powder grades," in *Proceedings of the Annual International Solid Freeform Fabrication Symposium*. Austin, Texas. 342-353, 2009.

5- Fridrun, P., "The influence of particle size distribution and surface roughness of carrier particles on the in vitro properties of dry powder" *Inhalations, Aerosol Science and Technology*, 31:4, 301-321, DOI: 10.1080/027868299304174.

6- Yongqing, F., Loh, N.L., Batchelor, A.W., Liu, D., Zhu, X., He, J., and Xu, K., "Improvement in fretting wear and fatigue resistance of Ti–6Al–4V by application of several surface treatments and coatings," *Surface and Coatings Technology*, 106.2-3, 193-97, 1998.

7- Matheson, K., Cross, K., Javahery, I., Plumb, J., and Spear, A., "Comparison of conventional open-cell aluminum foam and its additively manufactured twin," *MS & T 2016*, 745-52. 2016.

8- Wang, L., Li, H., Wang, F., and Ren J., Preparation of open-cell metal foams by investment cast. *China Foundry*, 2(1), 56-59. 2005.

9- Evans, A.G., Hutchinson, J., and Ashby, M., Multifunctionality of cellular metal systems. *Progress in Materials Science*, 43(3):171–221, 1998.

10- Wadley, H.N., Cellular metals manufacturing. *Advanced Engineering Materials*, 4(10):726–733, 2002

11- Kooistra, G.W., Deshpande, V.S., and Wadley, H.N.G., Compressive behavior of age hardenable tetrahedral lattice truss structures made from aluminium. *Acta Mater*. 52, 4229–4237, 2004

12- Murr, L.E., Gaytan, S.M., Medina, F., Martinez, E., Martinez, J.L., Hernandez, D.H., Machado, B.I., Ramirez, D.A., and Wicker, R.B., "Characterization of Ti-6Al-4V open cellular foams fabricated by additive manufacturing using electron beam melting," *Materials Science and Engineering*: A 527.7-8, 1861-868, 2010.

13- Bussu, G., and Irving. P., "The role of residual stress and heat affected zone properties on fatigue crack propagation in friction stir welded 2024-T351 aluminium joints," *International Journal of Fatigue* 25.1, 77-88, 2003.

14- Hironori, S., Tane, M., and Nakajima, H., "Fatigue crack initiation and propagation in lotus-type porous copper," *Materials Transactions* 49.1, 144-50, 2008.

15- Wohlers T.T, (2009) Wohlers report 2009: rapid prototyping & tooling state of the industry. Annual worldwide progress report. Wohlers Associates, Detroit.

16- Jacobs P.F. *Stereolithography and Other RP and M Technologies: From rapid prototyping to rapid tooling*. SME, New York, 2005.

17- Gibson, I, et al., *Additive Manufacturing Technologies 3d Printing, Rapid Prototyping, and Direct Digital Manufacturing*. 2nd ed., Springer Verlag, 2016.

18- Wong, K.V., and Hernandez, A., “A review of additive manufacturing,” ISRN *Mechanical Engineering*, vol. 2012, pp. 1–10., 2012, doi:10.5402/2012/208760.

19- 3D Systems Inc. (1989) Stereolithography interface specification. 3D Systems, Valencia.

20- Chen, C., Graf, G., and Rosen, D.W., "Design for additive manufacturing of cellular structures," *Computer-Aided Design and Applications* 5.5, 686-696. 2008

21- Alexander, P., “Part orientation and build cost determination in layered manufacturing,” *Computer-Aided Design*, 30 (5), 343-356.

22- Kolar, V.D., "Application of reverse engineering and rapid prototyping to casting," *ETD Archive.Paper* 432, 2008.

23- Thompson, W.B., Owen, J.C., and James de St. Germain, H., Technical report on “Feature-Based Reverse Engineering of Mechanical Parts”, University of Utah Technical Report UUCS-95-010 (revised), November 6, 1995.

24- Varady T., Martin R.R., and Cox J., “Reverse engineering of geometric models--an introduction,” *Computer-Aided Design*, Volume 29, Number 4, pp. 255-268(14), 1997.

25- Baumers, M., Tuck, C., Bourell, D.L. et al., “Sustainability of additive manufacturing: measuring the energy consumption of the laser sintering process,” *IMechE Part B: J Eng Manuf* 225:2228–!2239.

26- “Settling the Debate: CNC Machining vs. 3D Printing,” Bunty LLC - Custom Machined, Forged, Cast & Plated Parts, buntyllc.com/settling-the-debate-cnc-machining-vs-3d-printing/. http://buntyllc.com/settling-the-debate-cnc-machining-vs-3d-printing/

27- “Ultralight Cellular Materials.” Wadley Research Group - UVA, University of Virginia, www.virginia.edu/ms/research/wadley/celluar-materials.html.

28- Ying, L. Image Process of Cement Sample. University of Utah, 2018.

29- Ashby, M.F., et al. Metal Foams A Design Guide, UK, Oxford (2000).

30- “Electron Beam Melting - EBM Process, Additive Manufacturing.” Arcam AB, www.arcam.com/technology/electron-beam-melting/.

31- Tang, Y. (2002) Stereolithography (SL) cure modeling. Master’s Thesis, School of Chemical Engineering, Georgia Institute of Technology.

32- Blazdell, P.F. “Solid free-forming of ceramics using a continuous jet printer,” *J Mater Process Technol* 137:49–54, 2003

33- Sirringhaus, H., Kawase, T., Friend, R.H., Shimoda, T., Inbasekaran, M., Wu, W., and Woo, E.P., “High-resolution inkjet printing of all-polymer transistor circuits” *Science* 290:2123–2126, 2000.

34- Banhart, J., "Manufacturing routes for metallic foams," *Jom* 52.12, 22-27, 2000.

35- Larry, E., Jr., Valimet, Inc., Inspection certificate (private communication), 04 May 2016.

36- Wadley, H.N.G. "Multifunctional periodic cellular metals," *Philosophical Transactions of the Royal Society A: Mathematical, Physical and Engineering Sciences,* 364.1838, 31-68. 2006.

37- Pingle, S.M., Fleck, N.A., Deshpande, V.S., and Wadley, H.N.G., "Collapse mechanisms maps for the hollow pyramidal core of a sandwich panel under transverse shear, *International Journal of Solids and Structures*, 48, p. 3417-3430, 2011.

38- Reig, LucÃ-a, ConcepciÃ³n Tojal, David Busquets, and Vicente AmigÃ³. "Microstructure and mechanical behavior of porous Ti-6Al-4V processed by spherical powder sintering," *Materials* 6.10,4868-878, 2013.

39- Yang, D., and Hur., B "The relationship between thermal decomposition properties of titanium hydride and the Al alloy melt foaming process," *Materials Letters* 60.29-30, 3635-641. 2006.

40- Fang, Z.Z., Powder Metallurgy Class Lab Cooperative Work.2016, Salt Lake City, UT, University of Utah.

41- Oh, J.-M., Heo, K.-H., Kim, W.-B., Choi, G.-S., and Lim, J.-W. "Sintering properties of Ti-6Al-4V alloys prepared using Ti/TiH2 powders," *Materials Transactions* 54.1, 119-21. 2013.

42- Kopeliovich, D., "Materials engineering," Sintering of Ceramics [SubsTech], 22 Nov. 2014. www.substech.com/dokuwiki/doku.php?id=sintering_of_ceramics.

43- Yadroitsev, I., Selective Laser Melting: Direct Manufacturing of 3D-Objects by Selective Laser Melting of Metal Powders (LAP Lambert Academic Publishing, Saarbrücken, 2009).

44- BrÃ¸tan, Vegard, et al. "Industrialization of metal powder bed fusion through machine shop networking," *Procedia CIRP*, vol. 54, pp. 181–185., 2016. doi:10.1016/j.procir.2016.05.089.

45- Criales, L.E., and TuÄŸrul Ã–zel. "Temperature profile and melt depth in laser powder bed fusion of Ti-6Al-4V titanium alloy," *Progress in Additive Manufacturing*, vol. 2, no. 3, pp. 169–177., 2017, doi:10.1007/s40964-017-0029-8.

46- Ramachandiran, N., "What is the 'heat affected area' in welding?" Quora, 21 Nov. 2015, www.quora.com/What-is-the-heat-affected-area-in-welding.

47- "Polyhedron." *Wikipedia*, Wikimedia Foundation, 31 Oct. 2017, simple.wikipedia.org/wiki/Polyhedron.

48- Sanders, A., “Ti-6Al-4V implants,” Jan. 2016.

49- Kar, S., Searles, T., Lee, E., Viswanathan, G.B., Fraser, H.L., Tiley, J., and Banerjee R., “Modeling the tensile properties in β-processed α/β Ti alloys,” *Metall. Mater. Trans. A*, 37 (3), pp. 559-566, 2006.

50- Gibson, L.J., and Ashby, M.F., *Cellular Solids: Structure and Properties* (second ed.), Cambridge University Press, Cambridge (1997).

51- Haden, C.V., Collins, P.C., and Harlow, D.G., “Yield strength prediction of titanium alloys,” *JOM*, 67 (6), pp. 1357-1361, 2015.

52- Fei, C., Chandran, K.S.R., Kumar, P. “New approach to achieve high strength powder metallurgy Ti-6Al-4V alloy through accelerated sintering at β-transus temperature and hydrogenation-dehydrogenation treatment.” *Scripta Materialia*, vol. 130, 2017, pp. 22–26., doi:10.1016/j.scriptamat.2016.11.005.

53- Ravichandran, K.S. “A simple model of deformation behavior of two phase composites.” *Acta Metallurgica Et Materialia*, vol. 42, no. 4, 1994, pp. 1113–1123., doi:10.1016/0956-7151(94)90128-7.

54- Wu, G.Q., Shi, C.L., Sha, W., Sha, A.X., and Jiang, H.R., “Effect of microstructure on the fatigue properties of Ti-6Al-4V titanium alloys,” *Mater. Des.*, 46, pp. 668-674, 2013.

55- Zhang, X.-C., et al. “Failure mechanism and mode of Ti-6Al-4V alloy under uniaxial tensile loading: Experiments and micromechanical modeling,” Materials Science and Engineering: A, vol. 676, pp. 536–545., 2016, doi:10.1016/j.msea.2016.09.019.

56- Brenne, F., Niendorf, T., and Maier, H.J., “Additively manufactured cellular structures: impact of microstructure and local strains on the monotonic and cyclic behavior under uniaxial and bending load,” *J.Mater. Process. Technol.* 213, 1558–1564, 2013.

57- Lütjering, G., “Influence of processing on microstructure and mechanical properties of (α+ β) titanium alloys,” *Mater. Sci. Eng. A*, 243 (1), pp. 32-45, 1998.

58- Sieniawski, J., et al. “Microstructure and mechanical properties of high strength two-phase titanium alloys,” *Titanium Alloys - Advances in Properties Control*, 2013, doi:10.5772/56197.

59- Niinomi, M “Mechanical biocompatibilities of titanium alloys for biomedical applications,” *Journal of the Mechanical Behavior of Biomedical Materials*, vol. 1, no. 1, pp. 30–42, 2008.

60- Zhang, X., et al. “Porous Ti6Al4V scaffold directly fabricated by sintering: Preparation and in VivoExperiment,” *Journal of Nanomaterials*, vol. 2013, pp. 1–7., 2013. doi:10.1155/2013/205076.

61- Castleman, K.R., *Digital Image Processing*. 2nd ed. 1996, Englewood Cliffs, New Jersey: Prentice-Hall.

62- Russ, J.C., *The Image Processing Handbook*. 6th ed. 2011, CRC Press.

63- L. Chen-Luh. *Practical Image Process & Analysis*. 2017, Salt Lake City, UT, University of Utah.

64- Heinl, P., Müller, L., Körner, C., Singer, R.F., and Müller, F.A., “Cellular Ti-6Al-4V structures with interconnected macro porosity for bone implants fabricated by selective electron beam melting. *Acta Biomater*., 4, 1536–1544, 2008.

65- Drescher, P., et al. “An investigation of sintering parameters on titanium powder for electron beam melting processing optimization,” *Materials*, vol. 9, no. 12, p. 974., 2016, doi:10.3390/ma9120974.

66- Greaves, G.N., Greer, A.L., Lakes, R.S., and Rouxel. T., "Poisson’s ratio and modern materials," *Nature Materials*, 24 Oct. 2011.

67- Lakes, R. "Advances in negative Poisson's ratio materials," *Advanced Materials* 5.4, 293-96. 1993.

68- Lakes, R. S. “Foam structures with a negative Poisson’s ratio,” *Science* 235, 1038–1040, 1987.

69- Paramore, J. D., et al. “Hydrogen-enabled microstructure and fatigue strength engineering of titanium alloys,” *Sci. Rep.* 7, 41444, 2017. doi: 10.1038/srep41444 (2017).

70- Boyer, R., Welsch, G., and Collings, E.W. Materials Properties Handbook - Titanium Alloys. (ASM International, 1994).

71- ASTM. B348-10: Standard Specification for Titanium and Titanium Alloy Bars and Billets. (ASTM). doi: 10.1520/B0348 (2010).

72- Shin, D.H., et al. “Spheroidization of low carbon steel processed by equal channel angular pressing,” *Materials Transactions*, vol. 44, no. 8, pp. 1630–1635., 2003. doi:10.2320/matertrans.44.1630.